Journal of Non-Crystalline Solids: X 4 (2019) 100033

Contents lists available at ScienceDirect

Journal of Non-Crystalline Solids: X

journal homepage: www.journals.elsevier.com/journal-of-non-crystalline-solids-x

Challenges with vitrification of Hanford High-Level Waste (HLW) to borosilicate glass – An overview

Ashutosh Goel[a,*], John S. McCloy[b], Richard Pokorny[c], Albert A. Kruger[d]

[a] Department of Materials Science and Engineering, Rutgers, The State University of New Jersey, Piscataway, NJ, USA
[b] School of Mechanical & Materials Engineering and Materials Science & Engineering Program, Washington State University, Pullman, WA, USA
[c] Laboratory of Inorganic Materials, Joint Workplace of the University of Chemistry and Technology Prague, Technická 5, 166 28 Prague 6, Czechia, and The Institute of Rock Structure and Mechanics of the ASCR, v.v.i., V Holešovičkách 41, 182 09 Prague 8, Czechia
[d] U.S. Department of Energy, Office of River Protection, Richland, WA, USA

ARTICLE INFO

Keywords:
Nuclear waste
Borosilicate
Glass
Chemical durability
Crystallization

ABSTRACT

The Hanford site in Washington State houses ~56 million gallons of radioactive wastes stored in 177 underground tanks. The waste must be immobilized and permanently stored, and the plan is to separate the tank wastes into low activity waste (LAW) and high-level waste (HLW) streams. The U.S. Department of Energy is building a Waste Treatment and Immobilization Plant at Hanford site to separately vitrify these two waste streams in borosilicate glass using Joule-heated ceramic melters (JHCM). Although the process of nuclear waste vitrification seems to be well established, in practicality, it is faced with complex problems starting from the design of glass compositions, to processing in melters and long-term performance of the final vitrified waste forms. The article presents an overview of our current understanding of critical challenges related to the development and performance of HLW glasses.

1. Introduction

The Hanford site in Washington State is home to ~56 million gallons (~212 million liters) of radioactive and chemical wastes stored in 177 underground tanks. The wastes were generated as a result of 45 years of plutonium production in support of the U.S. defense programs [1]. The plutonium used in the world's first nuclear explosion (codenamed “Trinity”) at Alamogordo, New Mexico, in July 1945, and in the second atomic bomb (codenamed “Fat Man”) came from Hanford. Today the Hanford tanks contain ~60% of the reprocessing waste in storage in the U.S. The majority of the remaining is stored at the Savannah River Site (SRS) in South Carolina built during the 1950s [2]. Fig. 1 shows an image of single-shell tanks (SST), while Fig. 2 presents an image of double-shell tanks during their construction at the Hanford site in 1940s. Fig. 3 presents a schematic of the cross-section of a typical SST at Hanford, depicting layer–by–layer arrangement of radioactive and chemical waste. As per the current plan [3], the Hanford tank waste will be separated into two categories – (1) High-Level Waste (HLW), and (2) Low Activity Waste (LAW). A brief description of the two types of wastes has been presented below.

- High-Level Waste (HLW): The HLW is a highly radioactive material resulting from the reprocessing of spent nuclear fuel (SNF), including liquid waste produced directly in re-processing and any solid material derived from such liquid waste that contains fission products in sufficient concentrations. This is in conjunction with any other highly radioactive material that requires isolation according to the Nuclear Regulatory Council [4]. In the Hanford SST, HLW exists mostly in the form of sludge and salt cake (Fig. 3), rich in sodium and aluminum oxides, nitrates and hydroxides along with the significant concentration of transition metal oxides, for example, Fe_2O_3, Cr_2O_3, NiO, Cr_2O_3, and MnO.
- Low Activity Waste (LAW): The LAW should not be confused with the low level waste (LLW) as defined by the International Atomic Energy Agency (IAEA). Also known as “waste incidental to reprocessing (WIR)”, LAW is a radioactive material, resulting from the reprocessing of spent nuclear fuel, which the U.S. Department of Energy (DOE) has distinguished from HLW. It constitutes approximately 90 vol% of the total Hanford waste inventory. Because it meets certain criteria, WIR poses less risk (compared to HLW) to the health and safety of people and the environment, and therefore, does not need to be disposed of as HLW. While the NRC regulates LLW, the LAW is managed under the U.S. DOE's regulatory authority. Regarding its chemical complexity, the LAW is primarily the

* Corresponding author.
E-mail address: ag1179@soe.rutgers.edu (A. Goel).

https://doi.org/10.1016/j.nocx.2019.100033

Available online 07 August 2019
2590-1591/ © 2019 Published by Elsevier B.V. This is an open access article under the CC BY-NC-ND license (http://creativecommons.org/licenses/BY-NC-ND/4.0/).

Fig. 1. An aerial view of the single-shell tanks (SST) under construction at Hanford site C-Farm, c. 1944. A total of 149 carbon steel SST with a design life of 20 years were built during 1943–1964. C-Farm was the first of the Hanford's SST farms selected for waste retrieval. Radioactive and chemical waste was pumped from C-Farm's twelve 100-series tanks (530,000 gal each), and four smaller 200-series tanks (55,000 gal each), and was sent to newer, double-shell tanks. At the time of this writing, the farm has been completely retrieved. The waste will be subsequently sent to the waste treatment and immobilization plan for the vitrification.

Fig. 2. An image of the double shell tanks under construction, c. 1970s. The construction of 28 double-shell tanks, with capacities up to 4400 m^3 and design lives of 50 years, began in 1968.

supernatant liquid in the tank waste (Fig. 3) comprising aqueous solutions of Na^+, K^+, $Al(OH)_4^-$, Cl^-, F^-, NO_2^-, NO_3^-, and minor water soluble radionuclide species, for example, $^{99}TcO_4^-$, and $^{129}I^-$ [5,6].

The U.S. Department of Energy (DOE) is building a Tank Waste Treatment and Immobilization Plant (known as WTP) at an estimated cost exceeding $17 billion, covering 67 acres (~27 ha) of area at the Hanford site, to separately vitrify LAW and HLW in borosilicate glass at 1150 °C using Joule-heated ceramic melters (JHCM) [3]. Fig. 4 presents an aerial view of the WTP (under construction) showing the major facilities being constructed for the pre-treatment of nuclear waste followed by its vitrification into borosilicate glass. The vitrification of nuclear waste is expected to start no later than 2022. With two 10 m^2 (melt pool surface area) LAW melters and two 3.75 m^2 HLW melters (all including bubblers), the WTP will be, by far, the world's largest nuclear waste vitrification facility [7].

Since the cost of vitrifying radioactive waste is directly proportional to the volume of glass to be produced, it is therefore desirable to maximize the waste loading in the glass to decrease the overall volume, but without posing an unacceptable risk for the melter operation or long-term performance of the vitrified waste form. For this reason, the majority of the research effort in the last decade has been focused on designing advanced glass formulations with increased waste loadings.

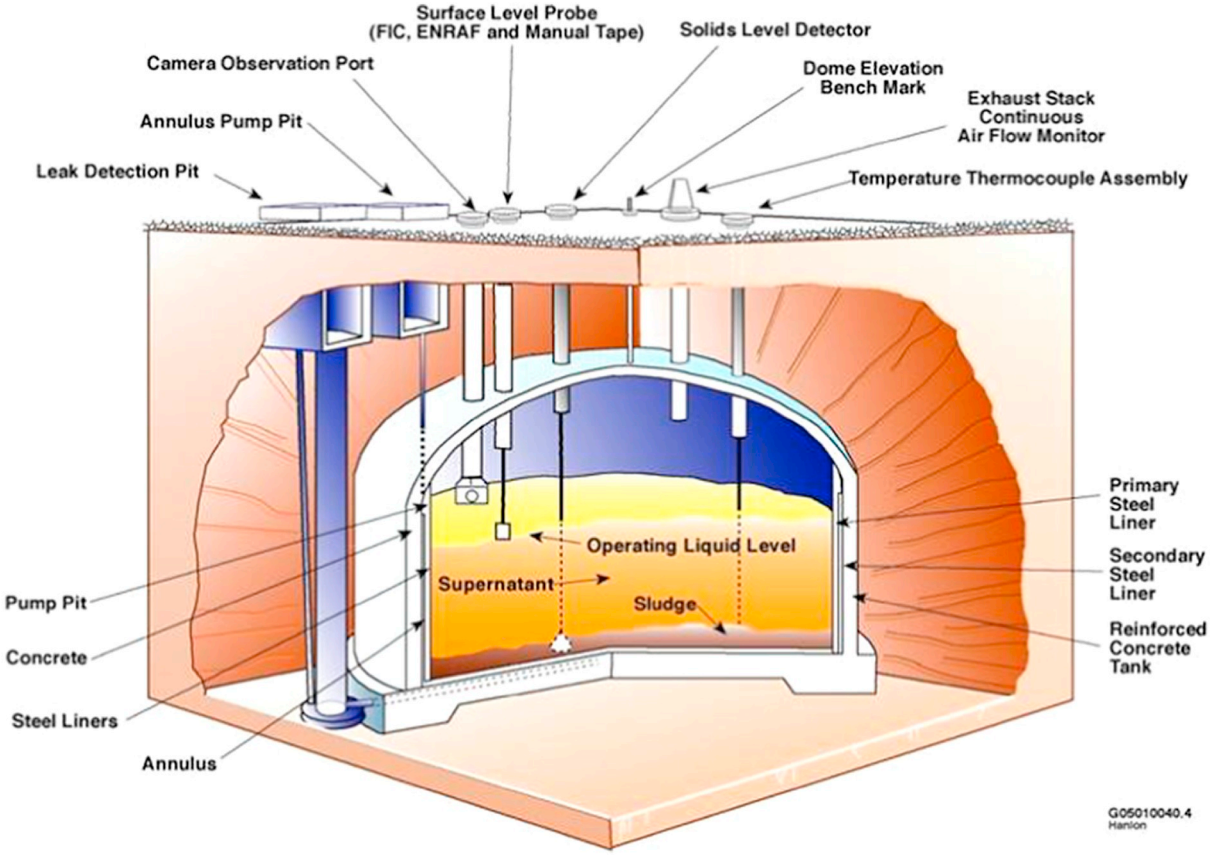

Fig. 3. A schematic of the layer–by–layer arrangement of the radioactive waste in a SST at the Hanford site.

As a result, a projected 30–50% reduction in the amount of glass and near tripling of melt rates has been achieved [7]. However, a further enhancement in the waste loadings is a challenge, considering that most of the current understanding in this field is based primarily on empirical data. Therefore, there is an exigent need to develop a solid fundamental understanding of the chemical, structural, and thermo-kinetic factors limiting the waste loading in the glassy waste forms. In this context, the current article aims to present an overview of current understanding of some critical challenges related to the development and performance of HLW glasses. This is followed by a set of open questions that need to be answered to understand the fundamental science of these glass systems and develop HLW vitrified products with higher waste loadings. It should be noted that the article is not intended as a thorough review of waste vitrification science and technology. It

Fig. 4. An aerial view of the WTP at Hanford site (under construction), c. 2018.

aims at highlighting various challenges with vitrification of Hanford's HLW into borosilicate glasses. For information about international experiences with the vitrification of nuclear waste, readers are suggested to follow these references [8-12].

2. Chemical complexity of the Hanford tank waste

The natural abundance of plutonium in nature is in trace quantities where it co-exists with ^{238}U deposits. Plutonium at Hanford site was generated by transmutation of uranium through irradiation of metallic fuel. The uranium fuel was, for the most part, cladded in aluminum, but one Hanford dual use (Pu production and power production) reactor used Zircaloy-clad fuel [13]. Three primary separations processes were used at Hanford to extract the ^{239}Pu. The first process, known as the Bismuth Phosphate Process (used for the fuel from B and T plants, 1944–1956), relied on sequential oxidation and reduction of soluble Pu (VI) to insoluble Pu(IV) co-precipitated with $BiPO_4$ or LaF_3 solids, depending on the process step. By controlled oxidation or reduction, combined with acidification or basification to promote the solid phase precipitation, plutonium was isolated from uranium, lanthanides, and other fission products [14–16]. At the same time that the bismuth phosphate process was operating, a new process, called REDOX, was developed and used to extract both plutonium and uranium at Hanford from 1952 to 1967. In REDOX, like other solvent extraction processes, Pu(VI) and U(VI) were extracted from a nitrate solution using liquid-liquid immiscibility of aqueous and organic phases, with methyl isobutyl ketone (MIBK) as the organic liquid. Subsequent addition of a reducing agent to the Pu + U mixture selectively reduced Pu to Pu(III) and allowed separation of U from Pu. PUREX was a solvent extraction method improvement over REDOX, where Tributyl Phosphate (TBP) in kerosene was used to extract 4+ and 6+ uranium and plutonium from a nitric acid aqueous solution of these actinides. After this development, some of the uranium from the $BiPO_4$ process waste was later recovered using the Tributyl Phosphate Process (1954–1958, known as the Uranium Recovery Process), and PUREX (Plutonium Uranium Redox Extraction) was implemented at the Savannah River Site at this time as well. Hanford began PUREX reprocessing in 1956, continuing on and off until 1990 [17,18].

All three processes ($BiPO_4$, REDOX, PUREX) operate based on the principle of changing oxidation state of Pu, thereby allowing selective decontamination and separation from elements with similar chemistry (uranium, lanthanides), as well as other fission products, fuel assembly constituents, corrosion contaminants, and process chemicals. Primary de-cladding and dissolution of the fuel was always performed with aqueous nitric acid, HNO_3. Therefore, the waste placed into the Hanford tanks is dominated by process chemicals (e.g., acids, NaOH for basification of the waste to protect the tanks), unrecovered solvents and their byproducts, and cladding metals (Al and Zr). Very little of the waste volume actually consists of radioactive elements, though some actinides including U, Pu, Am, Np, and Cm remain. The one exception is the remaining uranium-rich metal waste stream from the BPP [19].[1] The $BiPO_4$ process produced ~30 m^3 of waste per tonne of fuel, which is significantly more than the 2–15 m^3 produced by REDOX or 1–5 m^3 produced by the more efficient PUREX [7]. Final wastes were basified to pH 8 or higher, using sodium hydroxide and carbonate solutions, before being placed into one of the 177 steel-lined concrete tanks, with waste volumes ranging from ~0.2 to 4 million liters [20].

The waste volume, which had become excessive, was decreased by various processes, primarily water evaporation through different boiling techniques (for example, self-boiling, or by using in-plant and in-tank atmospheric evaporators and vacuum evaporators). Decontaminated water condensates were released to the ground, and concentrated salts were returned to the waste tanks [21]. The removal of such a large amount of water from the waste resulted in crystallization of various dissolved salts as salt cakes within the tanks, the dominant salt being $NaNO_3$. However, other single or double anion salts were also found in the tanks, for example, $Na_2C_2O_4$ (sodium oxalate), $NaAl(OH)_4$ (sodium aluminate), $Na_2CO_3{\cdot}H_2O$, NaF, $Na_7F(PO_4)_2$, Na_3FSO_4, and $NaAlCO_3(OH)_2$ [22–24]. In 1954–1958, the Waste Scavenging Process was implemented to remove and isolate the short-lived, high heat-producing isotopes $^{134,137}Cs$, ^{90}Sr, and ^{60}Co from secondary raffinates produced by the Uranium Recovery Process and similar wastes, and these fully decontaminated solutions were released to the environment [25].

The desire to remove theses short half-life soluble components from wastes continued in implementation of the Waste Fractionization Process (1967–1985). The remaining short-lived isotopes limited the volume reduction of the waste due to excessive heat load on the tank structures. Hence the remaining $^{134,137}Cs$ was removed by ion-exchange and $^{89,90}Sr$ was removed by solvent extraction. The collected Cs was formed to CsCl, and the collected Sr formed to SrF_2, and these salts were double-encapsulated and stored underwater, where they remain today, for heat dissipation and radiation shielding [8,26].

Depending on the process employed to separate ^{239}Pu, i.e., $BiPO_4$, REDOX, PUREX, as well as the detailed history of tank filling and blending, the following high-level waste streams have been generated, as delineated by statistical cluster analysis [27].

- Al, Fe, and Zr limited (tank AZ-101): Simultaneously high in aluminum, iron, and zirconium, as well as noble metals, these wastes will be very refractory and could benefit from higher melting temperatures were they available. With current Hanford glass formulation models, the waste loading is limited to 37%.
- Th and Zr limited (tank C-104): Containing refractory thorium and zirconium, this waste again will prove problematic for vitrification at high waste loading. However, it represents only a small fraction of the Hanford tank waste.
- Bismuth and Phosphorus limited: Primarily originating from the BPP, this waste represents a large volume for Hanford due to the inefficiency of $BiPO_4$ process and its generation of a relatively large waste volume. Phosphate solubility drives the waste loading, particularly in interaction with chromium [28–30].
- Chromium limited: This waste exists primarily due to the use of $Na_2Cr_2O_7$ as an oxidizer for Pu in the $BiPO_4$ and REDOX process. Other sources of Cr are from Cr(III) used to reduce permanganate and Cr from corrosion of the steel tanks [13]. It therefore constitutes large fraction of the Hanford tank sludge. Wastes containing Cr also usually contain a relatively high amount of SO_3, such as from chemicals added in the $BiPO_4$ process, including ferrous sulfate reductant and sulfuric acid for complexation of U(VI). Since both Cr and S are present together, waste loading may be limited to salt formation during melting, since Cr(VI) and S(VI) form oxyanions, chromate and sulfate and can partition with alkali in a molten salt.
- Aluminum limited: About half of the aluminum in the Hanford waste is from dissolved aluminum cladding, while the other half comes from aluminum nitrate used in the REDOX process [13]. The waste type and its variants constitute almost half of the Hanford HLW by mass.
- Aluminum and sodium limited: A subset of the high aluminum wastes exists where sodium is also present in high concentrations. Sodium is present due to the use of NaOH for removing the fuel cladding, as well as Na nitrate for hydrogen scavenging [13]. This waste case presents the worst-case scenario for nepheline crystallization (see Section 5.1).

[1] The inventory database maintained by the Hanford Site operations contractor estimates that approximately 6.5×10^5 kg of uranium is present in the Hanford tanks in the form of sodium urinates and uranium iron oxide complexes thus, making it the fourth most prevalent metal in the waste solids, after sodium, aluminum and iron. For further information, see Reynolds et al. [19].

Table 1
HLW compositions (wt%) from Hanford *(from Ref. [22], Courtesy: Battelle Memorial Institute)*.

Component	HLW					
	Fe, Al and Zr-Limited	Th and Zr-Limited	Bi and P-Limited	Cr-Limited	Al-Limited	Al & Na-Limited
Al_2O_3	24.58	9.69	23.18	27.48	52.95	45.13
B_2O_3	0.00	0.00	0.60	0.57	0.42	0.77
BaO	0.00	0.00	0.02	0.03	0.12	0.06
Bi_2O_3	0.00	0.00	13.33	7.85	2.53	2.45
CaO	1.40	1.67	1.66	2.66	2.38	1.53
CdO	2.16	0.27	0.00	0.01	0.05	0.02
Ce_2O_3	0.80	0.30	0.00	0.00	0.00	0.00
Cl	0.00	0.00	0.00	0.00	0.00	0.00
Cr_2O_3	0.46	0.40	1.03	3.30	1.15	1.50
Cs_2O	0.50	0.50	0.50	0.50	0.50	0.50
F	0.00	0.00	1.63	2.15	1.47	0.48
Fe_2O_3	37.67	17.80	13.83	14.13	13.03	5.95
HfO_2	0.00	14.35	0.00	0.00	0.00	0.00
K_2O	0.00	0.00	0.92	0.40	0.31	1.40
La_2O_3	0.89	0.00	0.00	0.00	0.00	0.00
Li_2O	0.00	0.00	0.32	0.39	0.38	0.16
MgO	0.00	0.00	0.85	0.17	0.26	0.46
MnO	0.91	3.55	0.00	0.00	0.00	0.00
Na_2O	10.58	11.03	13.39	21.62	7.91	26.88
Nd_2O_3	0.65	9.97	0.00	0.00	0.00	0.00
NiO	1.66	1.01	3.83	1.14	0.88	0.21
P_2O_5	1.34	1.37	9.91	3.59	2.32	4.27
PbO	0.00	0.00	0.50	0.52	0.90	0.19
Re_2O_7	0.00	0.00	0.00	0.00	0.00	0.00
RuO_2	0.15	0.10	0.10	0.10	0.10	0.10
SiO_2	3.77	6.57	12.43	11.36	10.81	6.48
SnO_2	0.66	0.00	0.00	0.00	0.00	0.00
SO_3	0.38	0.19	0.94	1.64	0.44	0.46
TiO_2	0.00	0.00	0.31	0.01	0.02	0.36
ZnO	0.00	0.00	0.32	0.27	0.18	0.38
ZrO_2	11.44	21.21	0.41	0.12	0.87	0.26

Table 1 presents representative chemical compositions (in oxides) of the above-mentioned waste streams.

3. The process of converting tank waste to borosilicate glass

Before discussing the challenges related to the development and performance of HLW glasses, it is crucial to understand the process resulting in conversion of waste to glass. The main steps in the vitrification process of nuclear waste are outlined below.

- Preparing the waste feed
- Mixing the waste with glass-forming oxides and other chemicals
- Feeding the mixture of waste + glass forming chemicals to the melter
- Heating the waste mixture to convert it into a melt
- Pouring the melt in steel canisters
- Treating the gaseous effluents from the melting process
- Cooling and decontaminating the filled canisters for storage and disposal.

As per the original plan, the tank waste will be separated into HLW and LAW at the pre-treatment facility. This will be followed by mixing of the respective wastes (LAW and HLW) with glass forming oxides and chemicals (for example, SiO_2, H_3BO_3, sucrose, etc.) Kg[2]. For the waste feeds rich in nitric acid, sucrose or oxalic acid is usually added as a reductant and to react with HNO_3 in the feed to form N_2 and CO_2 as described in the following reaction scheme.

$$20\,HNO_3 + 2\,C_{12}H_{22}O_{11} \rightarrow 10\,N_2 + 24\,CO_2 + 32\,H_2O + O_2$$

In reality, the reaction does not go to completion, and NO and NO_2 are generated from the reaction. A molar ratio of 10:1 between nitrate and sucrose has been found to be nearly an ideal ratio for the vitrification of Idaho sodium bearing waste, which is a representative of a high nitrate acidic waste vitrified in a liquid-fed test melter [31]. The mixtures will then be sent to JHCM (Fig. 5) where they will be heated in the temperature range of 1150–1200 °C to form molten glass. Fig. 6 presents a schematic overview of the vitrification process to be implemented at WTP in order to convert HLW and LAW to borosilicate glass. The glass melt will be poured into steel canisters. The LAW vitrification product will be disposed at the on-site Integrated Disposal Facility (IDF), while HLW glass will be transported to a deep geologic repository when such a location becomes available [32]. Owing to the large amount of water that is evaporated, and potential volatility of elements like ^{129}I and ^{99}Tc (primarily in LAW), a large part of the facility footprint is devoted to off-gas processing. Semi-volatile components captured in the initial off-gas scrub are recycled back to the melter.

4. Challenges during vitrification of HLW

4.1. Batch to glass conversion in the melter

The waste throughput rate, defined as [waste throughput rate] = [waste loading in glass] × [glass melting rate] is one of the primary concerns in the vitrification of radioactive wastes, because it directly influences the life cycle of nuclear waste cleanup [33]. While the next sections address the major effort conducted to design advanced glass formulations with enhanced waste loadings in glass, this section focuses on the glass melting rate. It provides an overview of the history of batch melting models, current state-of-the-art, and research questions addressed in support of the Hanford WTP.

Today, most glass furnaces, including waste glass melters, are optimized with the help of computational fluid dynamic (CFD) models to improve the melter energy efficiency, meet the required product criteria, or control the emissions. However, although the conversion of batch-to-glass has been studied for many decades to better understand the batch energy consumption, temperature field in the batch and the batch profile (width, length, thickness, shape), and the batch kinetics [34], only simplified empirical or semi-empirical models have been developed for the batch melting [35]. As a result, current CFD models still fail to accurately simulate this important, and usually rate-limiting process [36,37], and are of little-or-no-use for Hanford WTP where hundreds of feed compositions will be vitrified over the decades, exhibiting a broad range of melting behavior [38].

In a JHCM, the batch in the form of slurry (heterogeneous liquid mixture containing various solids) is charged from the top, creating a cold cap on the pool of molten glass that covers 90–95% of the melter surface. The one-dimensional models view the cold cap as a blanket of uniform thickness that receives steady uniform heat fluxes from both the molten glass below and the plenum space above. Fig. 7 shows a cold cap sample retrieved from a laboratory-scale melter [39–41]. Considering one-dimensional melting, each particle of the melter feed travels vertically down through the cold cap, experiencing increasing temperature in response to which its properties (for example, density, the dissolution rate of solids, reaction kinetics) are changing. The cold cap is composed of a reaction layer and a foam layer. While most of the heat is consumed in the reaction layer and during water evaporation from slurry at the cold-cap surface, the melting-rate-limiting step is the heat transfer through the foam layer, which forms at the cold-cap bottom where the glass-forming melt becomes continuous [41–43].

To enhance the heat transfer into the cold cap, forced convection is induced by bubbling gas into the melt [44,45], increasing the melting

[2] It should be noted here that at Savannah River Site, the HLW is mixed with borosilicate ground glass frit (instead of glass forming chemicals) and fed directly into the melter.

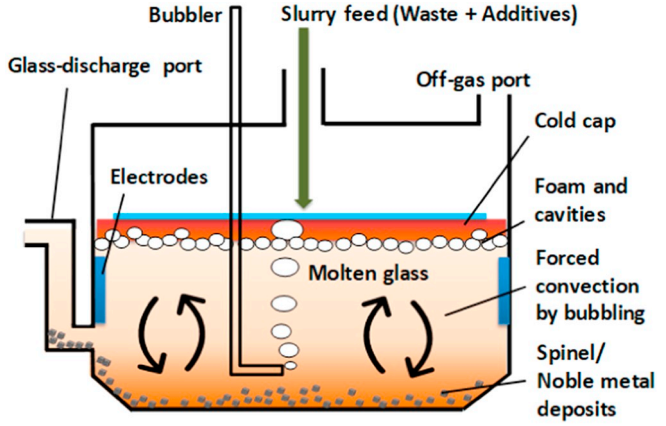

Fig. 5. Schematic cross-section of a JHCM presenting noble metals and spinel deposits in the HLW glass melter.

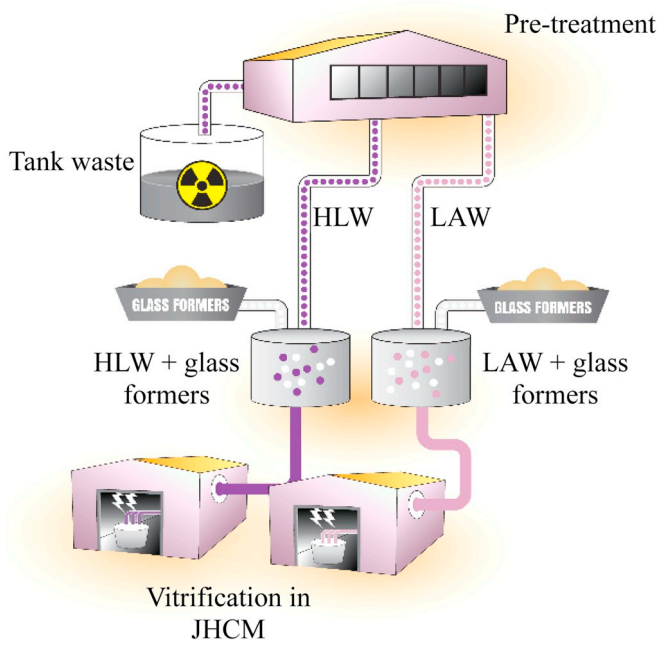

Fig. 6. Schematic of the vitrification process to be implemented at Hanford site.

rate by a factor of up to four [46]. This can be mostly attributed to the following factors: (i) an increased convection brings hot glass from the bottom of the melter to the vicinity of the cold cap, (ii) an increased fluid velocity decreases the thickness of the boundary layer near the bottom of the cold cap, and (iii) an increased convection and large bubbles from bubblers help to remove the insulating gas bubbles that form at the cold cap bottom from collapsing primary foam and from secondary bubbles ascending from the melt.

In the cold cap, the heat transfer is controlled by the heat conduction. Because conduction is a function of cold cap strucutre, it is affected by the kinetics of various chemical reactions and phase transitions that occur during the conversion process, especially those leading to the formation of foam at the cold-cap bottom. Thus, it is influenced by the choice of feed materials, including their mineral form and particle size. For example, varying the alumina source in feeds designed for high-alumina HLW vitrification [47–49] considerably affected the steady-state melting rates under the same melter operating conditions. A melting rate of 950 $kg\,m^{-2}\,day^{-1}$ has been reported for the feed containing gibbsite [$Al(OH)_3$] as the Al_2O_3 source, a melting rate of 1200 $kg\,m^{-2}\,day^{-1}$ for a feed with boehmite [AlO(OH)], and 700 $kg\,m^{-2}\,day^{-1}$ for a feed with corundum [Al_2O_3]. Similar effects

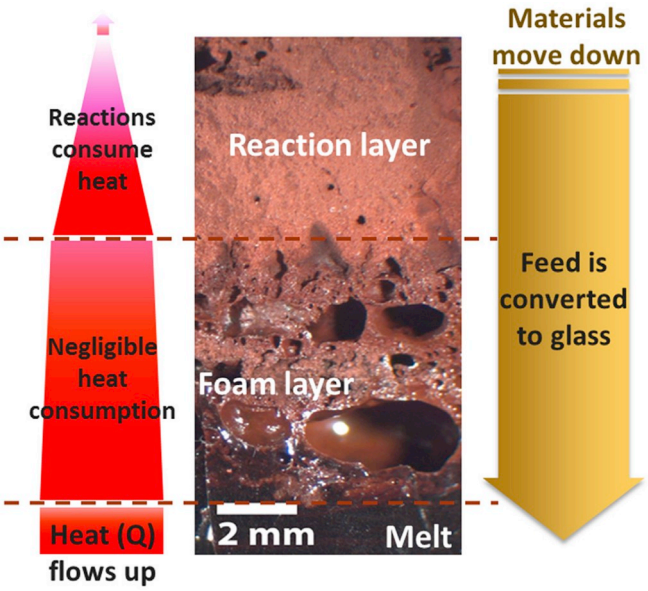

Fig. 7. Schematic of heat flux and feed movement in the cold cap (the cold-cap cross section was obtained from a laboratory-scale melter [39,40]). *Reprinted from* Lee et al. [41] *with permission from Elsevier*.

have been reported when varying the quartz particle size [33] or the source of iron [50].

In theory, the melting rate can be calculated using the cold cap heat transfer properties. While it is possible to measure or estimate those properties for the main reaction layer of the cold cap [51–53], simulating the heat transfer in the dynamic foam layer at the cold cap bottom is highly challenging – the heat transfer is affected not only by conduction and thermal radiation, but is dominated by the convection related to the growth, coalescence, and collapse of foam bubbles. As a result, it has not been possible to reliably estimate or measure the effective heat conductivity of the foam layer until now.

Thus, to predict the melting rate only as a function of feed properties and melter operating conditions while avoiding the calculation of heat transfer through foam, recent studies have focused on the understanding of the kinetics of foam evolution and collapse at the cold cap bottom [41,54–58]. While observing the real-time (in situ) foam behavior in the glass melters is still challenging [59,60], combining laboratory techniques such as the feed volume expansion test, evolved gas analysis, and thermogravimetry, allows to assess the important foam properties, such as foam onset and collapse temperature, foam porosity, or bubble size. The foam properties can be then used in the melting rate correlation (MRC) equation [57] and in the computational fluid dynamics model of the melter [61] to predict the rate of melting, having potential to (i) allow a rapid and reliable assessment of glass production/waste processing rate, (ii) help design and optimize the feed formulation, (iii) be useful for troubleshooting, and (iv) reduce time and cost by facilitating plans for the runs of experimental melters of various scales, which are time-consuming and expensive [62–66].

However, despite the significant efforts and progress that attracted the interest also from the glass industry [67–69], the understanding of batch-to-glass conversion is still far from complete. For example, the MRC has been, up to now, validated only for a relatively small range of HLW feeds in a pilot-scale melter. The validation for a broad range of HLW and LAW feeds is necessary, as well as its testing for melters of various scales. Also, better understanding of the structure-property relationship, i.e., the dependence of heat transfer on the formation and structure of foam is required. To that end, a more representative, but still practical model for the heat transfer in the foam layer has to be developed.

Another issue that still needs attention is the cold cap rheology

[70,71], i.e., the cold cap formation, spreading, and changes in its shape during melter operation. Although problems with cold cap formation are uncommon, the formation of shelf-like structures from hardened material or otherwise uneven cold caps with mounds and ridges are occasionally observed during testing in pilot-scale melters [48,72]. Such structures can prevent the feed slurry from spreading evenly, potentially leading to dangerous situations during the vitrification of actual radioactive waste when observation windows are not available to detect and resolve these situations in time, for example by decreasing the rate of slurry feeding or increasing bubbling rate from selected bubbler outlets. The use of non-visual data, such as plenum temperature, has not been developed yet as a reliable indicator of cold-cap conditions while processing the HLW feeds [73]. For example, high plenum temperatures can result from a high mound over a portion of the melt surface preventing feed from spreading across the melt surface and creating an opening on the glass surface. Without the visual evidence, an operator may conclude that feed rates should be increased, which could exacerbate the problem.

Finally, the issue with molten salts needs to be discussed. The molten salt phase, consisting mainly of inorganic salts used as sources of Na_2O and Li_2O and B_2O_3, is as fluid as water and, therefore, highly mobile. The primary melt easily wets surfaces of solids and molten glass while reacting with them. However, the possible excess of the primary melt over that which is immobilized by capillary forces (in liquid films and bridges) can migrate into porous areas or be drained by gravity [74,75]. The gravity-driven vertical migration of molten salt is not considered problematic, because the high-viscosity glass-forming melt becomes connected in the lower part of the cold-cap, creating a barrier for primary melt drainage. This barrier gives molten salts a chance to react with the rest of the cold-cap material, arguably at an even faster rate due to the higher temperature in the lower parts of the cold-cap. However, molten salt could also flow horizontally (e.g., at the cold-cap edges), leaving behind refractory components (mainly SiO_2, Al_2O_3, and ZrO_2) that could solidify into a frozen cold-cap [74]. This can be an issue during LAW feed vitrification, where the only solids will be minerals added as sources of the glass formers, and the amount of molten salts will be high [76,77].

4.2. Spinel crystallization in the glass melter

As discussed in Section 2, a major fraction of Hanford HLW is rich in oxides, hydroxides, and nitrates of sodium, aluminum, iron, nickel, chromium, and manganese, along with some noble metals. The presence of transition metal oxides (for example, Fe_2O_3, NiO, Cr_2O_3, MnO) in the waste feed pose a critical challenge for the lifetime and performance of the glass melter, thus impeding the waste loading in the vitrified waste form. In brief, one of the major factors limiting waste loading in HLW glasses is the precipitation, growth, and subsequent accumulation of spinel crystals $(Fe, Ni, Mn, Zn, Sn)^{II}(Fe, Cr)_2^{III}O_4$ in the glass discharge riser of the melter during idling (lowering the melter temperature to 850–900 °C when not in operation) [78–80]. Once formed, crystalline species such as spinels are stable to temperatures much higher than the typical JHCM operating temperatures (1150–1200 °C) [81]. Thus, spinel deposits, once formed, are difficult to dissolve [82]. This can result in clogging of the melter discharge channel and interfere with the flow of glass from the melter as shown in the schematic presented in Fig. 5 [78,83].

Historically, crystallization constraints – limiting the volume fraction of spinel in the glass melt to 1 vol% at 950 °C ($T_{1\%}$ at 950 °C) or designing glass compositions with liquidus temperature (T_L) lower than the melter operation temperature (T_M) – have been placed in compositional control systems to prevent premature or catastrophic failure of JHCM through bulk devitrification or crystal accumulation [84–87]. However, the validity of these constraints is now being challenged, as recent studies have suggested that significant increase in waste loading in HLW glasses are possible over current system planning estimates if a higher crystal content can be routinely processed in the HLW glass melters [88–90]. For example, an increase in tolerance limit of spinel concentration from 1 vol% to 2 vol% in the HLW glass melt can result in decrease of total glass volume to be produced by > 2000 MT [84]. Further, it has been shown that crystal contents as high as 4.2 vol% can be easily discharged through the Duramelter® DM-100 (smaller scaled HLW melter) after several days of idling at 950 °C [89].

Hanford flowsheets identified the $T_{1\%}$ constraint as one of the five most influential or restrictive constraints for estimated Hanford HLW glass volumes. For this reason, the U.S. DOE – Office of River Protection (ORP) has initiated a program to develop an appropriate and defensible crystallization control to modify or replace $T_{1\%}$ approach [88,89]. Therefore, the current effort on this topic is directed towards developing models to predict crystal accumulation (spinel settling) in the glass discharge riser as a function of the glass composition. In this pursuit, a preliminary empirical model (based on the spinel settling experiments in double crucible method [91]) has been proposed for predicting the compositional dependence of spinel crystal settling in the glass discharge riser of the HLW melter as shown in Eq. 1 [92].

$$h = \sum_{i=1}^{N} h_i x_i + t \sum_{i=1}^{N} s_i x_i \quad (1)$$

where, h is the thickness (μm) of the accumulated layer, h_i is the i-th component intercept coefficient (μm), t is the accumulation time (hours), s_i is the i-th component velocity coefficient (μm/h), x_i is the i-th component concentration (mass fraction), and N is the total number of components. While the model has been showing satisfactory results (in most cases) until now [91], there are four major challenges that need to be addressed to make this model more rigorous and to develop a holistic understanding about the compositional dependence of spinel crystallization in HLW glass melts.

(i) A typical HLW glass contains more than > 30 components. The current version of the model covers 17 of > 30 components, and that too in an un-optimized or partially investigated spectrum of compositions [91]. Therefore, more data about the compositional dependence of spinel crystallization in HLW glasses is required to improve this model.

(ii) There are glass compositions where spinel settling does not follow the behavior predicted by the model. For example, a recent study

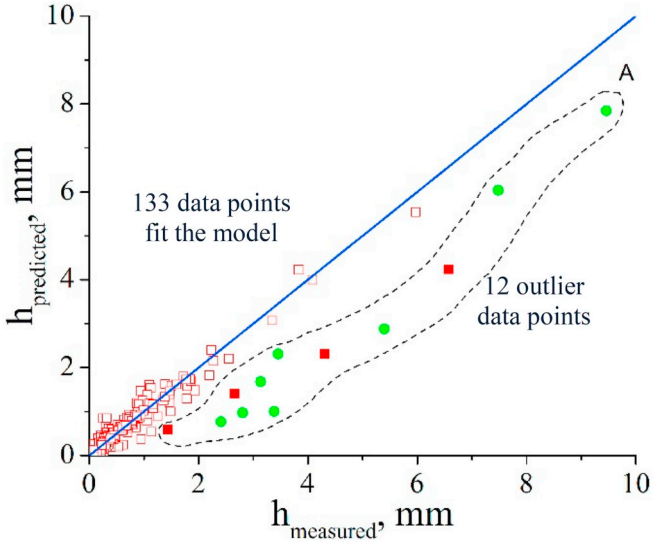

Fig. 8. Calculated vs. measured thickness of accumulated layers for 145 HLW glasses. *Reprinted from* Matyas et al. [91] *with permission from Elsevier.* A total of 133 out of 145 glass compositions fit the empirical model predicting the thickness of spinel layers at the bottom of glass melters.

has demonstrated that out of 145 HLW glass compositions tested using this model (Eq. 1), the settling behavior of spinel crystals of only 133 compositions could be predicted by the model accurately (Fig. 8), which can lead to potentially dangerous situations during radioactive melter operation. However, the model significantly underpredicted the settling behavior of spinels in the remaining 12 glass compositions [91,93]. This warrants an in-depth understanding of the crystallization behavior of these glasses and its impact on the rheology of the corresponding glass melts.

(iii) From the perspective of melter design, one of the critical parameters that must be fundamentally understood prior to implementing a crystal tolerant approach is the location and thickness of a crystal layer that is tolerable (i.e., the areas of the melter where crystals are likely to accumulate and the thickness of layers in those areas that is acceptable before a negative impact on the melter operation is expected).

(iv) Current understanding of the underlying compositional, structural and thermodynamic drivers controlling the nucleation and crystallization of spinels in HLW glass melts is poor. The knowledge and experience in this domain are crucial to design glass compositions with minimal tendency towards spinel crystallization in the HLW melter conditions. This is of high importance given the inability to inspect and service the WTP melter discharge riser based on the current design. Thus, the spinel crystallization and settling on the ledge in discharge riser and pour spout of the melter has to be avoided [84].

4.3. Noble metals in the glass melter

Generally, noble metals are defined as silver, gold, platinum, and the platinum group elements. These metals are characterized by a common property— chemical inertness. The platinum group metals (PGMs) comprise ruthenium, osmium, rhodium, iridium, palladium, and platinum. Of these, Ru, Rh and Pd originate from the fission of ^{235}U and are present in the U.S. defense HLW as a product from the reprocessing of irradiated fuel. As an example, Hanford neutralized current acid waste (NCAW) contains the radioactive noble metal isotopes listed in Table 2. Ruthenium is not only the most abundant noble metal in the Defense Waste Processing Facility (DWPF) [94] and Hanford HLW [95], but also has the most complex chemistry in borosilicate glasses. For example, Pd and Rh remain in metallic phases in the molten glass, whereas Ru can exhibit multiple oxidation states in glasses depending on the chemistry and redox behavior of the glass melt. For this reason, understanding Ru chemistry in borosilicate glasses is the most important among all the PGM for the vitrification of Hanford HLW [95].

Metallic ruthenium melts at 2310 °C and boils at 3900 °C, temperatures significantly higher than the operating temperatures of JHCM. Further, at ~800 °C, Ru oxidizes in air to form RuO_2. The reprocessing of nuclear fuel yields wastes that contain many different species of Ru, where Ru^{3+} nitrosyl derivates, for example, trinitrato nitrosylruthenium $[RuNO(NO_3)(H_2O)_2]$ or sodium tetranitro nitrosylruthenium, $Na_2[RuNO(NO_2)_4OH]$, are expected to be the most common ruthenium complexes in the Hanford waste [95]. Under highly oxidizing conditions, ruthenium can also occur as a gas with composition RuO_4. If produced in the HLW melters (which is rarely the case as Hanford HLW melters are expected to work under reducing atmosphere), the poisonous and radioactive RuO_4 gas must be either chemically trapped, removed by denitration of waste, or fixed by other chemical or physical methods. Although the denitration or the reduction of ruthenium from +8 oxidation state eliminates the production of gaseous RuO_4, it only reduces ruthenium volatilization by about one order of magnitude [96].

Table 2
Radioactive noble metals in NCAW *(from Ref. [90], Courtesy: Battelle Memorial Institute)*.

Isotope	Half Life	Stable Decay Product
^{103}Ru	39.3 days	^{103}Rh
^{106}Ru	372.6 days	^{106}Pd
^{102}Rh	2.9 years	^{102}Ru
^{103m}Rh	56.1 min	^{103}Rh
^{107}Pd	6.5×10^6 years	^{107}Ag

Although the compositional dependence of ruthenium solubility in borosilicate glasses is not well understood, it is known to be sparingly soluble in the glassy matrix with its solubility being in the range of few hundred parts-per-million by weight. According to Mukerji et al. [97], the oxidation state of ruthenium when dissolved in a glassy matrix depends on the basicity of the latter. Ruthenium was reported to dissolve as Ru^{3+} and Ru^{4+} in acidic silicate glasses, Ru^{4+} and Ru^{6+} in basic silicate glasses, Ru^{6+} and Ru^{7+} in soda phosphate glasses, Ru^{4+} and Ru^{6+} in lead phosphate and borophosphate glasses, and Ru^{3+} and Ru^{4+} in borosilicate glasses. Shuto et al. [98] studied the ruthenium solubility in a series of Na_2O–SiO_2, CaO–SiO_2 and Na_2O–Al_2O_3–SiO_2 glasses. It was reported that the ruthenium solubility increased with an increase in the oxygen partial pressure and content of basic oxides. However, it decreased with increasing temperature. According to Shuto et al. [98], Ru dissolved in the silicate glasses as an acidic oxide where the dissolution reaction is $Ru + 3/4O_2 + 1/2O^{2-} \rightarrow RuO_2^-$ and $\Delta H^o = -130 \pm 20$ kJ/mol. When present in +4 (RuO_2) and 0 (metallic Ru) oxidation states, ruthenium was insoluble or sparingly soluble in borosilicate glasses and is consequently observed as grains or needles dispersed in the glass, as shown in Fig. 9 [99–101]. Depending on their crystal size and morphology, the RuO_2 particles can either remain dispersed through the resulting glass melt or settle on the melter floor (due to their high density, 6.97 g/cm^3) thus causing a disruption in the flow of melt [94,95,102].

Individual and clustered RuO_2 particles can heterogeneously nucleate other phases, for example, nepheline ($NaAlSiO_4$), acmite, and spinel, in the glass melt [103]. RuO_2 is an effective nucleating agent in borosilicate glasses due to its low solubility, high melting point and high specific surface area. In terms of volatility, 2.8–7.5 wt% ruthenium volatility has been reported from borosilicate glass melts containing 0.05–0.15 wt% RuO_2 when subjected to a heat treatment at 1150 °C for 3 h.

Another major problem with RuO_2 crystallization in the glass melts is its high electrical conductivity ($s = 2.5 \times 104\,\Omega^{-1}\,cm^{-1}$). It has been shown that the electronic transport is responsible for the abnormally high electrical conductivity for RuO_2 content as low as 0.4 vol% in simulated HLW borosilicate glasses. Further, the electronic conductivity of RuO_2 in borosilicate glass matrices has been shown to

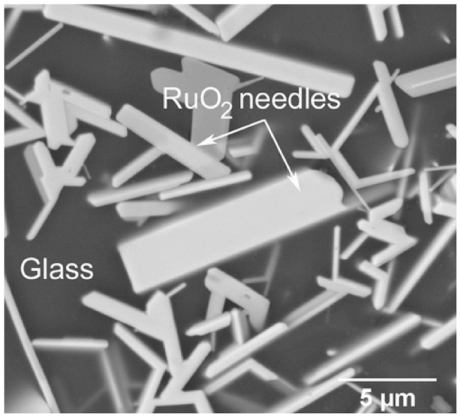

Fig. 9. SEM image of a sodium borosilicate glass containing RuO_2 after heat treatment at 1300 °C followed by quenching to room temperature. *Reprinted with permission from* Boucetta et al. [101]. *Copyright (2012) American Chemical Society.*

depend not only on its concentration in the glass–RuO_2 composite, but also on the ruthenium solubility in the glassy matrix, the organization of the RuO_2 particle network, and the size and morphology of the RuO_2 particles [104,105].

Almost all the major waste vitrification facilities (research or production) around the world have experienced different levels of operational problems that can be traced to the presence of noble metals in the melters. In the U.S., the possibility of settling of noble metals on the HLW melter floor, and its adverse impact on the HLW vitrification, was not fully appreciated before the design of the DWPF melters had been completed and construction had started on the first two melters. Therefore, as part of the Hanford Waste Vitrification Project (HWVP), the studies were performed during the 1980s comparing the melter designs of flat-bottomed, side electrodes design (DWPF melter design) to the slope-bottomed with bottom electrodes [106]. The liquid used to simulate molten glass was glycerin with 7.5 wt% LiCl. Noble metal particles were represented by nickel and silica. The slope-bottomed model exhibited enhanced convection currents due to bottom electrodes. However, both models performed about the same regarding maintaining particles in suspension. The data indicated that if the noble metals had a density of 12 g/cm^3 (Pd/Rh) and if their size were $<$ 40 μm, only 1% of the incoming noble metals would settle under steady-state melter operating conditions. In the size range of 40–60 μm, 10% particles will settle, and for sizes up to 100 μm, 50% of the noble metal particles will settle in the melter. According to the experiments simulating melter idling, the noble metal particles up to 40 μm in size will completely settle on the melter floor in ~30 days. Further, these studies also suggest that a bubbler operating in the full-scale melter at 8 scfh[3] will be ineffective at either re-suspending noble metals in the size range of 40–100 μm, or keeping them in suspension. For smaller particle sizes, the bubbler was shown to be effective but the results were inconsistent [95].

Several attempts have been made to find a solution to the problem of accumulation of noble metals in the glass melters. Igarashi and Takahashi [107] proposed to decrease the temperature at the bottom of the slope-bottomed melter to slow down the precipitation of noble metals, and to modify the design of the bottom drain to improve the discharge performance of the noble metals. However, control over noble metal accumulation may become challenging with an increasing burn-up of the fuel, as in fast reactors. Therefore, an efficient and safe removal of noble metals prior to final waste vitrification is a better option to ensure a continuous and stable vitrification process. In this context, the majority of the research (by researchers mainly from India and Japan) on this topic has focused on removal of noble metals either from the HLW prior to vitrification [108–113], or from the borosilicate glass melts during vitrification using different metals as alloying agents [114,115]. In the U.S., recommendations have been made to modify the insulation and heaters to introduce more convection currents during idling, and to allow for physical stirring or bubbling of the melts. Further, a systematic parametric variation study using both experimental and computational techniques has been recommended to establish a comprehensive understanding of the behavior of noble metals in borosilicate glass melts [95]. It should be noted that the JHCMs being installed at Hanford WTP are flat bottomed with two side discharge systems and no bottom drain. The slope-bottomed JHCMs have been used at the German Waste Vitrification plant (VEK) and are also being installed at Rokkasho, Japan and Lanzhou, China [3].

4.4. Direct feed HLW

In order to begin the treatment of the nuclear waste as soon as possible, the U.S. DOE is considering the possibility of implementing a sequenced approach for vitrification of LAW and HLW at the Hanford site. The sequenced approach is called direct feed LAW (DFLAW) and direct feed HLW (DFHLW). If brought into practice, this approach will begin the treatment of LAW by 2022. In the LAW direct feed option, the LAW from tank farms will be directly sent to the LAW vitrification facility. For DFHLW the pretreatment facility could be bypassed in order to support an earlier start-up of the vitrification facility. For the HLW, this would mean that the ultrafiltration and caustic leaching operations that would otherwise have been performed in the pre-treatment facility would either not be performed or would be replaced by an interim pretreatment function (for example, in-tank leaching and settling) [116,117]. Simultaneous advances in waste loading of aluminum can obviate the need for caustic leaching of HLW. This has an added benefit of significantly reducing the inventory of soda reporting to LAW. The proposed changes in the processing of both LAW and HLW waste streams are likely to affect glass formulations and waste loadings and have impacts on the downstream vitrification operations. In particular, three potential major challenges during vitrification of DFLAW and DFHLW are expected to be (1) high concentration of alkali/alkaline-earth sulfates, phosphates and chromates in waste melter feeds which could lead to salt formation on the melt surface, (2) high concentration of fluoride salts in DFHLW if the waste is not properly washed before sending it to the melter, and (3) corrosion of K-3 refractory in the melter due to high alkali and alkaline-earth content in the waste feed leading to reduction in the melter lifetime.

4.4.1. Models to constratin sulfur loading in DFHLW glasses

Historically, the HLW was supposed to be pre-treated for the removal of sulfate prior to vitrification. Therefore, sulfur loading in HLW glasses was not considered to be a potential problem. The recommended model to constrain sulfate (SO_3) loading in HLW glass is given by Eq. (2) [118]:

$$w_{SO_3}^{Limit} = \sum_{i=1}^{p} S_i n_i + S_{Li_2O \times Li_2O} n_{Li_2O}^2 \quad (2)$$

where ${w_{SO_3}}^{Limit}S_i$ is the i^{th} component coefficient given in the reference [118], $S_{Li_2O \times Li_2O}$ is the coefficient for normalized Li_2O concentration squared, and n_i is the ith component concentration in the glass normalized to 1 after removing SO_3: $n_i = {g_i}/{1 - g_{SO_3}}$, where g_i is the ith component mass fraction in the glass. On the other hand, the waste loading limitations in Hanford LAW glasses have been largely driven by solubility of sulfur in the melt, as melt feeds with excess concentrations of sulfur will form an alkali- and alkaline-earth rich sulfate molten salt layer that will accumulate on the melt surface. The salt creates several potential problems associated with melter operation as have been highlighted by Vienna et al. [119].

In order to avoid the potential problems due to the introduction of alkali and alkaline-earth sulfates in the DFHLW, the glass melters should be operated in a way to avoid salt accumulation. Avoiding salt formation in the melters requires either (1) conservative empirical limits on salt-forming components such as sulfur, chromium, and halides, or (2) a model able to predict the practical limit of salt solubility in the melter as a function of melter feed composition. The current understanding about sulfur incorporation in nuclear waste glasses is limited to LAW vitrification.

For example, based on the compositional dependence of sulfur solubility in LAW glass melts, Mueller et al. [120] had proposed a 20-term partial quadratic mixture model to relate sulfate solubility to LAW glass composition using a dataset of 370 WTP-LAW and ORP-LAW glasses. This model has been recently revised to a 31-term partial quadratic mixture model using a data of 485 WTP-LAW and ORP-LAW glasses [121]. The model is based on the measured sulfate solubility in the glass in wt% directly, without transformation, with sulfate solubility varying between 0.15 and 1.83 wt%.

While these empirical composition – property models have been successful in design of LAW glasses with suitable waste loadings, it will

[3] scfh: standard cubic feet per hour.

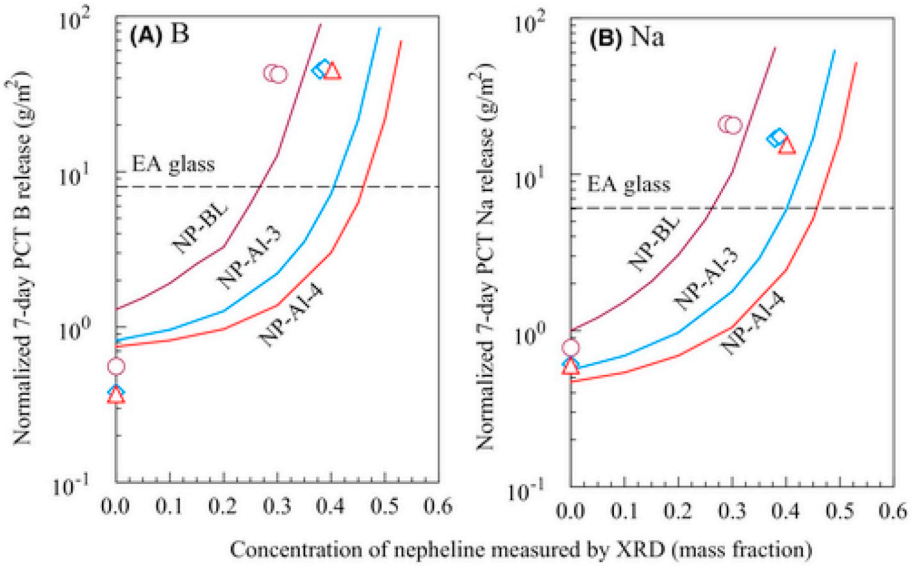

Fig. 10. Impact of nepheline precipitation on the normalized release of (a) boron and (b) sodium from HLW glasses after 7 days in PCT. *Reprinted with permission from* Vienna et al. [130]. *Copyright (2016) The American Ceramic Society and Wiley Periodicals, Inc.*

be difficult to design glass compositions for DFHLW using these models owing to the complex chemistry of sulfur in the multicomponent borosilicate based nuclear waste glasses [122–124]. In fact, it has been shown that the present sulfate solubility models based on LAW glass compositions do not perform well with the HLW glass data [120]. The range of many constituents in HLW glasses is also quite different from that in LAW glasses. Furthermore, the number of HLW glasses with sulfate solubility data is not enough for model development. Thus, more data needs to be collected to support the development of models that relate sulfate solubility in HLW glasses with their chemical compositions.

4.4.2. Fluoride salts in DFHLW glasses

A part of the 56 million gallons of HLW at Hanford site was generated from stripping of zircaloy cladding from the spent nuclear fuel rods by dissolving them in NH_4F/NH_4NO_3 solutions via Zirflex process followed by neutralization with NaOH [22]. Accordingly, zircaloy cladding is approximately 50% NaF by mass. The current plan is to wash this waste with water to dissolve the soluble fluoride salts, for example, NaF, Na_3FSO_4, and $Na_7F(PO_4)_2{\cdot}19H_2O$ [125]. While the dissolved salts will be blended with other low radioactivity wastes prior to disposal, the zirconium in the zircaloy waste will be vitrified [22].

According to our estimate, ~55 million gallons of water may be required to dissolve all the fluoride salts from just one tank at Hanford site (for example, AW-103). Therefore, it may be an arduous task to remove all the fluoride salts from the DFHLW before they are sent for vitrification. As per our knowledge, there is minimal literature addressing this problem until now. Thus, a dedicated effort is required to understand the factors controlling the fluoride solubility in HLW glasses and to develop a model constraining the fluoride loading in DFHLW glasses.

4.4.3. Refractory corrosion

The second major problem with the implementation of the DFHLW approach is the potential for K-3 refractory corrosion. Monofrax™ K-3 is a high-Cr_2O_3 refractory where the dominant phase is a complex solid solution of various spinels [126]. The spinel phases are mixtures of the four end-member spinels (Mg, Fe)O·(Al, $Cr)_2O_3$ and some SiO_2 [127,128]. This refractory is being used in Hanford's HLW and LAW glass melters. In particular, as the alkali content is increased, K-3 refractory corrosion rates tend to increase, which can result in decreased melter lifetime [120].

Current understanding of the mechanisms governing the corrosion of K-3 refractory in nuclear waste glass melter is highly limited [127,128], as the majority of the studies performed on this topic have been confined to measurements of dimensional loss of refractory material when in contact with glass melt in accordance with ASTM C621 [120,121]. While these tests have resulted in development of a 28-term partial quadratic mixture model to correlate K-3 refractory corrosion neck loss with the LAW glass composition, using a dataset of 344 WTP-LAW and ORP-LAW glasses, it does not provide any information about the chemical, thermodynamic and kinetic parameters controlling these corrosion reactions. For example, based on this empirical model, it has been shown that K-3 corrosion is severely increased by Li_2O, Na_2O, K_2O, and CaO present in the glass composition, whereas, glass components like Cr_2O_3, Al_2O_3, V_2O_5 and SiO_2 are beneficial in reducing the refractory corrosion [121]. Similarly, the batch make-up and redox behavior of glass melt have been shown to exhibit considerable impact on K-3 refractory corrosion [128]. Further, with introduction of alkali sulfates, chromates, and phosphates in DFHLW melter feed, K-3 refractory corrosion may be a potential limiting factor for design of these glasses with enhanced waste loadings. However, the actual mechanisms controlling these reactions are still unknown. An understanding of reaction pathways leading to corrosion of K-3 refractory in DFHLW glass melters can pave the path to optimize the glass compositions and melter conditions for suppression of this corrosion.

5. Performance-based issues with the HLW glass

5.1. Nepheline crystallization

Nepheline is a rock-forming tectosilicate mineral with an ideal composition $Na_6K_2\ Al_8Si_8O_{32}$. It is by far the most abundant of the feldspathoids, with its TO_4 (T = Si, Al) framework consisting of the single six-membered (S6R) tetrahedral building unit typology as in tridymite (hexagonal polymorph of SiO_2), but with half of the Si^{4+} cations replaced by Al^{3+} cations. Nepheline crystallization in sodium- and aluminum-rich HLW glass melts (during their cooling in the steel canisters) is a major concern, as it can result in severe deterioration of the chemical durability of the final waste form (as assessed by Product Consistency Test – PCT [129]) since each mole of nepheline ($Na_2O{\cdot}Al_2O_3{\cdot}2SiO_2$) removes three moles of network forming oxides (1 Al_2O_3 and 2 SiO_2) for one mole of non-framework cation (for example, Na_2O, Li_2O or K_2O).

Table 3
CCC heat treatment schedule. *Reprinted (and adapted) with permission from* Vienna et al. [125]. *Copyright (2016) The American Ceramic Society and Wiley Periodicals, Inc.*

Start temperature (°C)	Cooling rate (°C/min)
1050	1.556
980	0.806
930	0.591
875	0.388
825	0.253
775	0.278
725	0.304

Fig. 10 demonstrates the impact of nepheline crystallization on the chemical durability of HLW glasses in terms of the normalized release of boron and sodium from glasses in PCT after 7 days. Superimposed on the figure is boron PCT response for the DWPF environmental assessment (EA) glass limit [130]. Therefore, to meet the current disposal requirements, nepheline precipitation in HLW glasses must be avoided or the amount of nepheline formed and its impact on PCT must be predicted. Since the canistered glass will be subjected to a broad range of thermal histories, simulated canister centerline cooling (CCC) is used as a bounding thermal history to determine the risk of nepheline formation. Table 3 presents the CCC treatment schedule generally followed during the conversion of HLW melt-to-glass by controlled cooling.

An intensive effort has been made in past two decades to develop a constraint that avoids the composition regime prone to nepheline formation without unduly limiting the waste loading of HLW glass. Accordingly, five models have been proposed that aimed to predict the propensity of nepheline crystallization in HLW glasses as described below.

5.1.1. Nepheline discriminator (ND) model

The ND model was proposed by Li et al. [131] to identify the glass compositions that may have high susceptibility towards nepheline crystallization. The model was developed based on an extensive experimental dataset demonstrating that nepheline is unlikely to crystallize outside of its primary phase field in the ternary Na_2O–Al_2O_3–SiO_2 sub-mixture phase diagram. It is based on limiting the normalized SiO_2 concentration (N_{Si}) by the inequality as shown in Eq. (3).

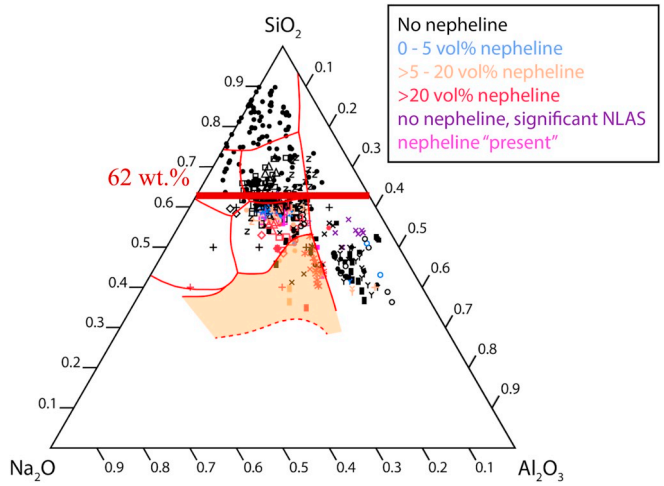

Fig. 11. The Na_2O–Al_2O_3–SiO_2 submixture ternary (wt%) of 629 HLW glasses. *Reprinted from* McCloy et al. [133] *with permission from Elsevier.*

$$N_{Si} = \frac{g_{SiO_2}}{g_{SiO_2} + g_{Al_2O_3} + g_{Na_2O}} < 0.62 \quad (3)$$

where g_i is the ith component mass fraction in the glass. The inequality equation (Eq. (3)) divides the nepheline and albite ($NaAlSi_3O_8$) primary phase fields in the Na_2O–Al_2O_3–SiO_2 ternary phase diagram as seen in Fig. 11.

Although the ND model has been incorporated into the predictive models for Hanford [123] and the DWPF [132], it is overly conservative. According to a recent study by Vienna et al. [130], the maximum Al_2O_3 concentration attained in realistic Hanford HLW glasses while complying with ND model is 18.3 wt%, suggesting that the ND model is too conservative with respect to the waste loading. As is evident from Fig. 11, many glass compositions with $N_{Si} < 0.62$ do not crystallize nepheline upon CCC treatment [133]. The lower N_{Si} glasses are those with the higher waste loadings. Further, the ND model does not account for the impact of network formers and non-framework cations (other than Na_2O, Al_2O_3 and SiO_2) on the tendency towards nepheline crystallization in HLW glasses. For example, P_2O_5 and B_2O_3 are known to exhibit a significant impact on the structure of aluminosilicate glass network, thus affecting their crystallization behavior [131,134–136]. Recent results on the crystallization behavior of nepheline-based glasses in the systems Na_2O–Al_2O_3–B_2O_3–SiO_2, and Na_2O–Al_2O_3–B_2O_3–P_2O_5–SiO_2 (mol.%) demonstrate that both B_2O_3 and $P_2O_5 \geq 10$ mol% are effective in suppressing nepheline crystallization in these glasses [137,138]. Similarly, the redox chemistry of iron is known to play a significant role in nepheline crystallization in HLW glasses as has been shown in our recent publications [139–141]. Therefore, a less conservative method of limiting nepheline crystallization is needed to both maintain acceptable glasses and allow higher waste loading.

5.1.2. Optical basicity (OB) model

The OB model was proposed by McCloy et al. [1,142] as a revised constraint whereby glasses with $N_{Si} < 0.62$ would show minimal tendency towards nepheline crystallization provided the optical basicity of the melt was < 0.55. The OB model was based on the hypothesis that more basic cations are more likely to cause aluminosilicates to precipitate, as they readily donate valence electrons and thus can be readily removed from the covalent glass network. Eq. (4) presents the formula for calculating the OB of glasses.

$$\Lambda_{glass} = \frac{\sum_i x_i q_i \Lambda_i}{\sum_i x_i q_i} \quad (4)$$

where q_i is the number of oxygen atoms in the ith component oxide, x_i is the ith component oxide mole fraction, and Λ_i is the ith oxide molar basicity.

It should be noted that the OB model was not introduced to replace the ND constraint. Instead, the aim was to use the OB model as a supplementary metric along with the ND model to bin those glasses which fail the ND criterion ($N_{Si} < 0.62$), but do not precipitate nepheline or other aluminosilicate phases during CCC treatment. Accordingly, a Cartesian quadrant system was created based on the threshold criteria (ND = 0.62 and OB = 0.575) (as shown in Table 4) where every glass can be represented by an (x, y) pair of (ND, OB). The threshold value of OB = 0.575 was chosen empirically by examining a set of glasses including simulated SB5 DWPF-like glasses and other HLW glasses rich in alkali and alkaline-earth oxides [1].

Table 4
Cartesian quadrant system created for nepheline discriminator (ND) and optical basicity combinations. *Reprinted with permission from* McCloy et al. [1]. *Copyright (2011) The American Ceramic Society and Wiley Periodicals, Inc.*

II: ND high enough, OB too high	I: ND too low, OB too high
III: ND high enough, OB low enough	IV: ND too low, OB low enough

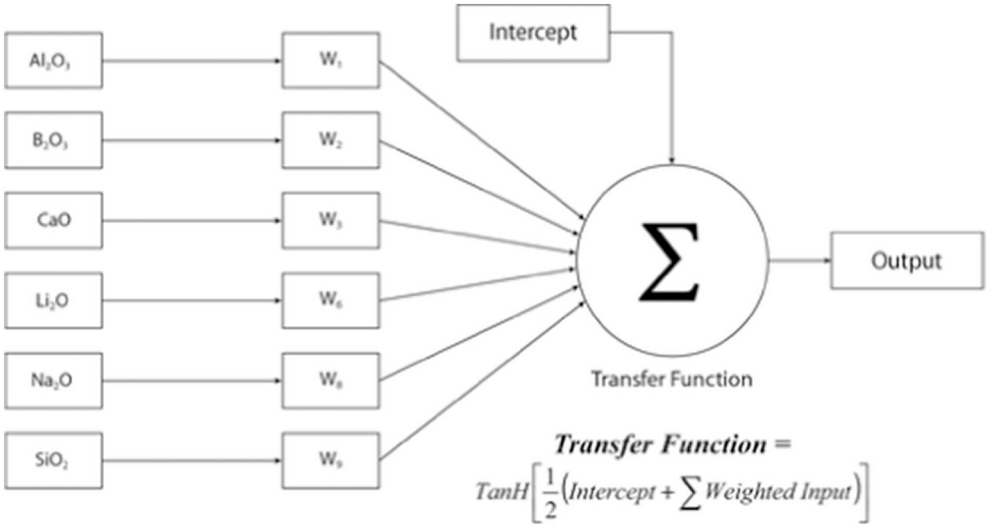

Fig. 12. Node diagram from neural network (*from Ref.* [118], *Courtesy: Battelle Memorial Institute)*.

The concept of OB has been useful in explaining the reason for why substituting B_2O_3 (OB = 0.40) for Al_2O_3 (OB = 0.61) is more effective in suppressing nepheline crystallization in the $25Na_2O–25Al_2O_3–50SiO_2$ glass, in comparison to substituting B_2O_3 for SiO_2 (OB = 0.48). The impact of P_2O_5 (OB = 0.40) on the nepheline crystallization in Na_2O-Al_2O_3-B_2O_3-SiO_2 system can be explained based on the same hypothesis. However, the case of substituting CaO for Na_2O is still debatable. As per the OB model, increasing CaO/Na_2O ratio in a HLW glass should suppress its tendency towards nepheline crystallization owing to the lower OB of CaO (OB = 1.0) in comparison to Na_2O (OB = 1.11). However, the test results on the crystallization behavior of (25- *x*)Na_2O–*x*CaO–$25Al_2O_3$–$50SiO_2$ glasses demonstrate a minimal impact of varying Na_2O/CaO ratio on their propensity towards nepheline precipitation [143]. It is worth mentioning that the glass system investigated is highly simplified in comparison to a typical nuclear waste glass. Therefore, it may not be a true representative of a complex HLW glass. Further, the maximum Al_2O_3 concentration attained in realistic Hanford HLW glasses while complying with the OB or ND constraints has been calculated to be 24 wt%, suggesting that OB model is also too conservative.

5.1.3. Neural network model

A neural network model was developed using the data from 629 glasses available at that time [113]. The approach estimated the probability of nepheline formation and was selected because it could account for highly non-linear interactions between the components. The model comprised a network with single layer and three nodes, all using the hyperbolic tangent (tanh) activation function. These nodes were classified as the hidden layers of the model. An example node is presented in Fig. 12. A series of modeling experiments explored the effects of many different glass descriptors, including OB, and ND, and un-normalized mass fractions of Al_2O_3, B_2O_3, CaO, Fe_2O_3, K_2O, Li_2O, MgO, Na_2O and SiO_2. It was determined that the normalized component concentrations and OB were not as effective in predicting nepheline formation as the un-normalized oxide concentrations.

In order to create the most predictive model possible, K-fold cross validation was used. This method splits the data set into *k* subsets. Each of these subsets contain 1/(1-*k*) of the data for modeling as well as a unique 1/*k* of the data for validation. Each of these subsets is modeled and the best model based on validation performance is presented. With K-fold validation, it is possible to evaluate the predictive properties of the model by retaining a portion of the data during the modeling of each subset. During the development of this model, *k* was varied from 5 to 628 and efforts were made to create a quantitative prediction model for the nepheline fraction in glass, but the data points were not enough to create an accurate model. As a result, a binary response (i.e. nepheline forms or not) was modeled and the misclassification rate (Eq. 5), as well as a weighted model score (Eq. (6)), were used to qualify the model.

Actual Result

Test	+	-
+	True Positive	False Positive
-	False Negative	True Negative

Experimentally Formed Nepheline

Predicted to Form Nepheline	Yes	No
Yes	True Positive 147 (23%)	False Positive 32 (5.1%)
No	False Negative 11 (1.7%)	True Negative 439 (70%)

Fig. 13a. Model scoring (a) nomenclature, and (b) summary for the selected nepheline neural network model (*from Ref.* [118], *Courtesy: Battelle Memorial Institute)*.

$$Misclassification\% = \frac{Number\ of\ incorrect\ predictions}{Total\ number\ of\ predictions} \quad (5)$$

$$Weighted\ Model\ Score = \frac{True\ Positives \times 2.7142 + True\ Negatives}{Positives \times 2.7142 + Negatives} \quad (6)$$

The results from this model relied on classifying each glass into one of the four categories as shown in Fig. 13a. The test result was classified as positive or negative. Actual nepheline response and predicted nepheline response were compared, and if they matched, the data point was classified as true. Therefore, a glass that is predicted to form nepheline is a positive, and it becomes true positive if the composition actually forms nepheline. Fig. 13b summarizes the outcome of each of the 629-glass dataset as per the developed neural network model. The

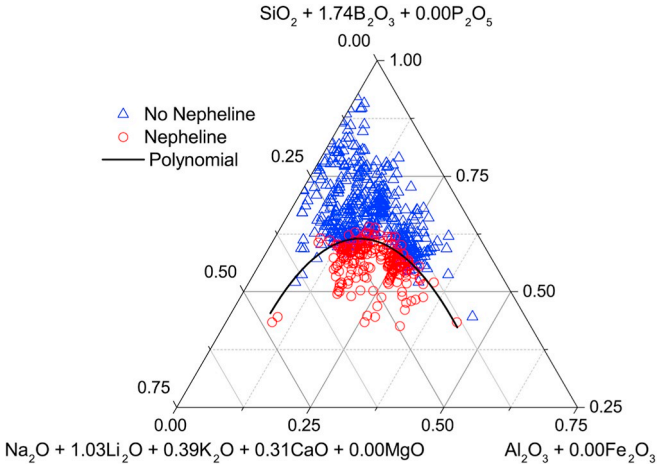

Fig. 14. Pseudo-ternary phase diagram with polynomial curve to separate glasses that form nepheline from those that do not. *Reprinted with permission from* Vienna et al. [130]. *Copyright (2016) The American Ceramic Society and Wiley Periodicals, Inc.*

as developed neural network model is an initial attempt to define a composition region in which nepheline is likely to form. The next steps include expansion of dataset and development of a method for quantifying the prediction uncertainties of such a model, which will be difficult as this model involves complex calculations requiring 25 coefficients, as documented by Vienna et al. [118,130].

5.1.4. Sub-mixture model

The sub-mixture model is the most recent model developed by Vienna et al. [130] to predict nepheline crystallization in HLW glasses. The model is an extension of the ND model that accounts for the potential impacts of those components that have been theorized to impact nepheline formation in waste glasses, for example, alkali and alkaline-earth oxides, network forming oxides (B_2O_3, P_2O_5) and Fe_2O_3. Accordingly, a pseudo-ternary phase diagram has been constructed comprising alkali and alkaline-earth oxides (Li_2O, Na_2O, K_2O. MgO, CaO) as one pseudo-component; Al_2O_3 and Fe_2O_3 as the second pseudo-component; and SiO_2, B_2O_3 and P_2O_5 as the third pseudo-component. The data pertaining to nepheline crystallization during CCC tests in 657 simulated HLW glasses (from the literature) and 90 new glass compositions has been used to construct this pseudo-ternary phase diagram. The following two different approaches have been used to construct the pseudo-ternary.

a. Polynomial Discriminating Curve – Submixture Model (PDC–SM)
b. Logistic Regression (LR) – Submixture Model (LR – SM)

In the PDC–SM approach, multicomponent HLW glasses were projected onto a submixture ternary followed by the fitting of a polynomial curve to the experimental data to partition the ternary into two regions based on the presence or absence of nepheline after CCC. On the other hand, the LR–SM approach is based on the same submixture ternary idea as the PDC–SM approach but uses a logistic regression for predicting the nepheline crystallization after CCC. The LR–SM approach was found to be more practical for predicting nepheline crystallization in HLW glasses as it uses all the data points to fit the model, whereas the PDC–SM approach uses only the data points that misclassify nepheline formation to fit the model. Hence, the PDC–SM approach assigns zero weights to the glass compositions for which the nepheline formation is correctly classified. On the contrary, the LR–SM approach uses all data points (with equal weights) and is then able to predict the probability of nepheline formation for any HLW glass composition (whether used to fit the model or not). Therefore, the latter has been recommended by Vienna et al. [144] for predicting nepheline formation in HLW glasses. For further details about PDC–SM and LR–SM approaches, refer to the technical report by Vienna et al. [144].

Fig. 14 presents an example of such a ternary pseudo-diagram with fit parameters optimized to reduce the sum of the squared distances between misclassified data points and a second-order polynomial shown in the plot. A total of 747 data points (657 from the literature and 90 new) have been plotted in the pseudo-ternary, where the 212 glasses that formed nepheline during CCC have been shown in red circles, while the 535 glasses that did not form nepheline have been shown in blue triangles. The general trend in data suggests that the method is a more precise predictor of nepheline formation than either the ND or OB constraints, and is more predictive than the neural network model. Further, according to the submixture model, P_2O_5, Fe_2O_3 and MgO have an insignificant effect on the nepheline crystallization in HLW glasses. Vienna et al. [130] attributed this observation to the limited concentration ranges of these oxides in the HLW glasses or precipitation in other crystalline phases, for example, magnetite. Recent studies describing the impact of Fe_2O_3 and P_2O_5 on nepheline

Table 5
Glass compositions designed in the crystallization phase field of nepheline along with their ND and OB values, crystallization heat treatment/cooling schedule and their propensity towards nepheline crystallization.

Glass	Li_2O	Na_2O	CaO	Al_2O_3	B_2O_3	Fe_2O_3	P_2O_5	SiO_2	ND	OB	Crystallization schedule	Nepheline crystallization	Reference
BL	–	25	–	25	–	–	–	50	0.42	0.608	950 °C, 24 h	Yes	[143]
NC-5	–	20	5	25	–	–	–	50	0.44	0.605	950 °C, 24 h	Yes	[143]
NC-10	–	15	10	25	–	–	–	50	0.46	0.602	950 °C, 24 h	Yes	[143]
NC-15	–	10	15	25	–	–	–	50	0.49	0.599	950 °C, 24 h	Yes	[143]
SC-5	–	25	5	25	–	–	–	45	0.40	0.624	950 °C, 24 h	Yes	[143]
SC-10	–	25	10	25	–	–	–	40	0.37	0.642	950 °C, 24 h	Yes	[143]
Li-5	5	20	–	25	–	–	–	50	0.44	0.601	Cooling of melt from 1500 °C to room temperature	Yes	[148]
Li-10	10	15	–	25	–	–	–	50	0.46	0.594		Yes	[148]
Li-15	15	10	–	25	–	–	–	50	0.49	0.587		Yes	[148]
Li-20	20	5	–	25	–	–	–	50	0.51	0.581		Yes	[148]
SB-10	–	25	–	25	10	–	–	40	0.37	0.590	950 °C, 24 h	Yes	[137]
SB-20	–	25	–	25	20	–	–	30	0.31	0.574	950 °C, 24 h	Yes	[137]
BA-10	–	25	–	15	10	–	–	50	0.49	0.576	850 °C, 24 h	Yes	[137]
BA-20	–	25	–	5	20	–	–	50	0.59	0.545	850 °C, 24 h	No	[137]
AF-0	–	25	–	20	10	–	–	45	0.43	0.583	700 °C, 1 h	Yes	[141]
AF-2.5	–	25	–	17.5	10	2.5	–	45	0.45	0.590	700 °C, 1 h	Yes	[141]
AF-5	–	25	–	15	10	5	–	45	0.47	0.597	700 °C, 1 h	Yes	[141]
AP-0	–	25	–	25	10	–	–	40	0.37	0.590	900 °C, 24 h	Yes	[138]
AP-5	–	25	–	20	10	–	5	40	0.40	0.567	900 °C, 24 h	Yes	[138]
AP-10	–	25	–	15	10	–	10	40	0.44	0.546	800–850 °C, 24 h	No	[138]

crystallization in model HLW glasses support the predictions made by the submixture model. Fe_2O_3 has a significant impact on the mechanism and kinetics of crystallization in $NaAl_{(1-x)}Fe_xSiO_4$ based glasses [139,140]. However, it exhibits an insignificant impact on promoting nepheline crystallization in $NaAl_{(1-x)}Fe_xSiO_4$ – B_2O_3 glasses [141]. Similarly, P_2O_5 tends to suppress nepheline formation in model HLW glasses in the system $25Na_2O$–$25Al_2O_3$–$10B_2O_3$–$40SiO_2$ (mol.%) in concentrations ≥10 mol%, which is considerably higher than that present in a typical HLW glass (0–3 mol%) [138].

5.1.5. Thermodynamic modeling of nepheline crystallization in HLW glasses

This effort is focused on developing a thermodynamic database of HLW glasses with a goal of characterizing the equilibrium behavior of nepheline and related phases in these systems. Accordingly, thermodynamic evaluation of the Na_2O–Al_2O_3–SiO_2 and Na_2O–Al_2O_3–B_2O_3–SiO_2 glass systems has been made by assessing the pseudo–binary and –ternary systems formed from Na_2O, Al_2O_3, B_2O_3 and SiO_2, for example, Na_2O–B_2O_3, B_2O_3–Al_2O_3, B_2O_3–SiO_2, Na_2O–Al_2O_3, Na_2O–B_2O_3, Na_2O–SiO_2, Na_2O–B_2O_3–SiO_2, Al_2O_3–B_2O_3–SiO_2 and Na_2O–Al_2O_3–SiO_2 systems [145–147]. The calculations of phase diagrams (CALPHAD) methodology using the two–sub-lattice partially ionic liquid (TSPIL) model, and compound energy formalism (CEF) has been employed to characterize the equilibrium behavior of the solid solutions and liquid phase, respectively [145–147]. This effort is still in its early stages and more work needs to be done to predict the compositional dependence of nepheline crystallization in HLW glasses.

5.1.6. A comparison of ND, OB and SM models – an example

Table 5 presents a set of 20 exemplary glass compositions with their ND and OB values. If we consider ND values as the criterion for predicting nepheline crystallization, all the compositions presented in Table 5 are expected to crystallize nepheline. However, at least two glasses, i.e. BA-20 and AP-10 do not crystallize upon prolonged heat treatments at their expected crystallization temperatures as shown in Table 5. The inability of ND model to predict nepheline crystallization in these two glass compositions may be attributed to the fact that the ND model does not account for any other glass constituent except Na_2O, Al_2O_3 and SiO_2. Therefore, the impact of B_2O_3 and P_2O_5 on the glass structure and crystallization has been neglected. Further, if we combine the OB model along with ND, it can successfully predict the formation of nepheline formation in all the glasses. For example, all the glasses

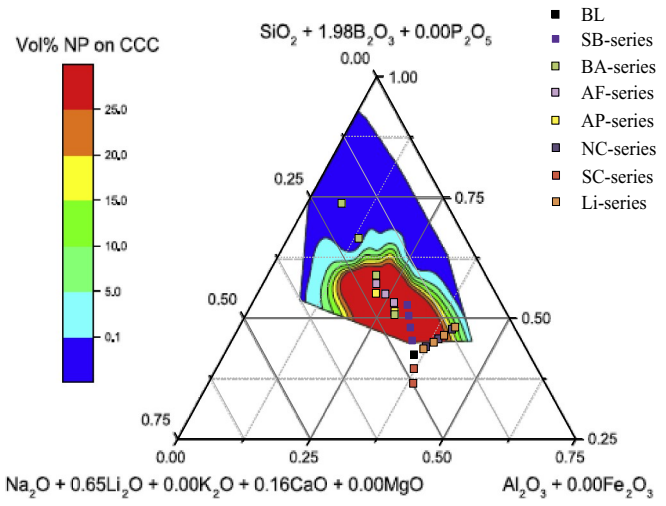

Fig. 15. Glass compositions from Table 5 plotted on a pseudo-ternary phase diagram with surfaces representing different volume percent of nepheline formed during CCC (using conservative fit). *The pseudo-ternary diagram has been reprinted with permission from* Vienna et al. [130]. *Copyright (2016) The American Ceramic Society and Wiley Periodicals, Inc.*

except BA-20 and AP-10 exhibit an OB value higher than 0.55. Therefore, they are expected to crystallize nepheline or other alkali/alkaline-earth aluminosilicate phases upon heating or during CCC. Although a combination of OB and ND models have been able to predict the nepheline crystallization in the compositions presented in Table 5, there are several other glass compositions where both ND and OB models fail to predict the crystallization behavior [130].

Fig. 15 presents the compositions from Table 5 plotted on a submixture ternary system predicting their tendency towards nepheline formation during CCC. One major advantage of the SM model over its analogues is that it cannot only predict the presence or absence of nepheline crystallization in HLW glasses, but it can also estimate the change in the concentration of nepheline crystallization with respect to change in the glass composition. For example, the SM model not only successfully predicted the minimal tendency of nepheline crystallization in BA-20 glass, but it could also successfully predict the trend of nepheline formation with respect to change in the Al_2O_3/B_2O_3 ratio in BA series vs. SiO_2/B_2O_3 ratio in SB series of glasses. A major challenge with SM model is that it does not account for the impact of P_2O_5 and Fe_2O_3 on the crystallization of nepheline in HLW glasses. For example, as per the experimental results, the glass AP-10 shows minimal tendency towards crystallization. However, the SM model cannot predict this result. Another challenge with SM model is the lack of enough experimental dataset to predict the nepheline crystallization in glasses over a broad composition space. For example, as can be seen from Table 5 and Fig. 15, there are several glass compositions (SC-series, BL glass) which tend to crystallize nepheline (or its polymorphs) but their behavior cannot be predicted by the SM model as these compositions lie outside the predictive region of the SM model.

5.2. Chemical durability of HLW glasses

Assuming that waste can be mixed into an adequately formulated glass, vitrification can be accomplished using robust practices, and deleterious crystallization can be avoided on cooling, the nuclear waste glass package must then be emplaced and stored in repository. Hanford HLW will ultimately be stored in a deep geological repository, while Hanford LAW will be emplaced in a shallow repository near the WTP vitrification facility. Regardless of the repository condition, eventually (after ~1000 years, depending on the conditions) the steel canister surrounding the glass will corrode and lose integrity. Groundwater may then interact with the glass itself, and through a series of processes, radionuclides may release into the environment. Thus, the stability of glass nuclear waste forms in the presence of groundwater represents the last line of defense in establishing a controlled release of radionuclides to the biogeosphere.

Since natural glasses which are relatively unaltered can still be found with ages > 1 billion years [149,150], it is feasible to believe that there are conditions and compositions which allow highly durable glass to exist on the earth. However, since glass by definition is a thermodynamically metastable phase, its ultimate fate is crystallization to more stable phases [151], a process which is generally accelerated by interaction with water The chemical durability of glass, particularly with respect to water, is generally described as the field of glass corrosion or glass alteration, the two terms being sometimes used interchangeably and sometimes emphasizing certain processes. Much of the research on glass degradation is motivated by the need to understand and quantitatively predict the release of radionuclides contained in nuclear waste glass under conditions relevant to geological repositories. The predicted release of radionuclides drives the safety assessment of these repositories. It is thus highly desirable to obtain mechanistic models which predict glass dissolution and alteration as a function of glass composition and environment [152].

Nuclear waste glasses of greatest concern are HLW borosilicate glasses with compositions significantly different than natural glasses produced by earth processes. However, some natural glasses like

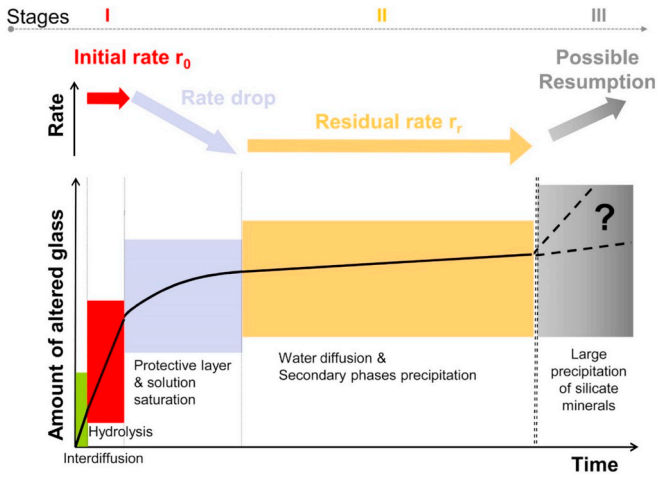

Fig. 16. Stages of nuclear glass corrosion and related potential rate-limiting mechanisms. The duration of each stage depends on glass composition and leaching conditions (temperature, pH, composition, renewal rate of the solution, etc.). *Reprinted from* Gin et al. [151] *with permission from Elsevier.*

basaltic glass have been used as proxies for borosilicate glasses due to their availability for study at various ages [153]. Water diffusion rates in both borosilicate and basaltic glasses are very low, with effective diffusion coefficients ranging 10^{-17}–10^{-23} $m^2 s^{-1}$, with quantified variations due to temperature (e.g., 25–90 °C), pH (e.g., 3–10), and glass composition [154–156]. Since the water diffusion rate is so low, alteration of glasses is seen primarily as a surface reaction.

Glass alteration proceeds in three sequential named phases or stages which vary considerably in their time dependence (as shown in Fig. 16). *Stage I* is the initial rate or forward rate of alteration of the pristine glass. *Stage II* is the residual rate, much lower than the initial rate. In some cases, a *Stage III* also exists, where a fast alteration rate resumes after a period of low alteration rates [144]. Most researchers agree that the initial dissolution rate (*Stage I*) can be described by the hydrolysis of Si—O—M bonds (M = Si, Al, Zr, Fe, Zn, etc.) and some interdiffusion [152,157] (except a few [158,159]).

Several mechanisms seem to compete during the *Stage II* residual rate, however, which may be the most important for geological disposal as the initial rate proceeds to the residual rate in very short times [160,161]. Multiple important phenomena are evident in tests of the residual rate, including water (or hydronium) diffusion into the pristine glass through ion exchange, water transport limitations due to a passivating layer within a forming amorphous gel [162,163] and slow transformation of gel layers into more stable crystalline phases [164]. All of these processes depend on local solution conditions (e.g., dissolved species concentration, solution renewal frequency, pH) so different tests produce different results for the same glass, and some may be more relevant than others for particular repository conditions. This complexity hampers scientific consensus on the relative significance and even interrelationship among these geochemically influenced alteration mechanisms [165–168]. Thus, depending on the conditions, *Stage II* alteration may be thermodynamically limited, reaction (kinetically) limited, or transport (kinetically) limited.

The difficult-to-predict resumption of rapid alteration (*Stage III*) in some glasses at various times in their alteration pathway constitutes a more problematic source for modeling, as all the mechanisms are less well-defined than for *Stage II*. In general, however, the appearance of *Stage III* seems to depend on glass composition as well as evolving near-field solution environment. *Stage III* alteration involves the appearance of crystalline phases consuming ions from the solution, the gel, and/or the glass, and can often be promoted by high temperatures and very alkaline (pH > 10) solutions [169–171].

Considering these factors, it is apparent that the design of a robust chemically durable nuclear waste glass requires detailed understanding of compositional and environmental dependence of mechanisms controlling both *Stage II* and *Stage III* alteration. A thorough understanding of water and ion transport into porous solids (rearranged gel and relict 'hydrated glass') is needed. The role of aqueous species concentration is needed as is influences concentration dependent diffusion as well as precipitation effects due to heterogeneous nucleation of crystalline phases on the gel [152]. Some questions are posed below which have focused and are focusing the glass alteration community towards greater understanding.

(i) What are the rate limiting mechanisms of the residual rate? What are the most important parameters influencing the residual rate? Readers should refer to the following articles to understand the current state-of-the-art on this topic [158,159,166–168,172].

(ii) It is now known that, under specific conditions, dissolution can suddenly resume at low rates, especially when zeolite crystalline phases precipitate (*Stage III*). This phenomenon is difficult to predict. It is believed that the thermodynamic modeling of corrosion in borosilicate glasses can help identify glasses that could transform into zeolites, while a better understanding of kinetics of such transformation can help to make reliable kinetic predictions. Therefore, in order to make progress on this topic, the research needs to be performed to answer the following questions:
   a. How does zeolite precipitation trigger the resumption in alteration?
   b. Will the dissolution rate be maintained until the complete alteration of glass?
   c. How does *Stage III* glass corrosion depend on the glass composition?

(iii) The relationship between glass composition and alteration rate is not straightforward, and elements which are advantageous in slowing rates in one process may be deleterious and accelerate rates in other processes. For example, Zn^{2+} slows down the initial dissolution rates but increases the residual rates [173]. Similarly, other minor constituents of HLW glasses, for example high ionic field strength cations [174], have been shown to exhibit significant impact on the mechanism and kinetics of glass corrosion. Therefore, it becomes imperative to understand the impact of glass composition on their kinetics and mechanism of corrosion.

(iv) What is the impact of near field materials in the vicinity of glass surface on the chemical durability of the waste form? It has been shown that magnetite or other iron oxide phases like hematite or goethite in contact with HLW glass can enhance glass dissolution, presumably due to precipitation of iron silicates which consume Si in the near-field solution and the gel [175–177]. In the case of Hanford HLW glass, in several instances, iron oxide phases partition out on the glass surface during CCC forming a crystalline surface layer [141]. However, the impact on chemical durability of such an iron oxide layer on the glass surface is not yet well understood.

6. Summary and concluding remarks

The U.S. DOE Office of Environmental Management is responsible for the nearly 100 million gallons of radioactive and complex liquid waste, most resulting from plutonium production during World War II and the decades after. A large fraction of this high-level "defense legacy" waste is currently stored at Hanford site in Washington State. The U.S. DOE must treat and dispose this waste, and the technology selected is vitrification using borosilicate glass. Previous and current U.S. vitrification operations, including the DWPF in South Carolina have shown the viability of this technology. As more experience has been gained in vitrifying the range of different wastes, new challenges and opportunities for improvement have been identified in waste-vitrification processes. The article presents an overview of the challenges that

are anticipated during the processing and long-term performance of HLW glasses at Hanford. Although great strides have been made in understanding the root-cause of these challenges, further research and development effort is required through collaborations between the U.S. national laboratories, universities and international partners to address the open questions and finding solutions to these problems. A dedicated effort in this direction will not only help to improve the efficiency of nuclear waste melters, but will also help to reduce the volume of glass to be produced and managed, thus, lowering the overall cost of the mission and safeguard the environment.

Declaration of Competing Interest

The authors declare that they have no known competing financial interests or personal relationships that could have appeared to influence the work reported in this paper.

Acknowledgements

This research was performed using funding received from the DOE Offices of Nuclear Energy (Nuclear Energy University Program) and Environmental Management (Office of River Projection), contract No. DE-NE0008597, 89304017C-EM000001, DE-EM-0003207 and 89304018CEM000006. Richard Pokorny acknowledges the support from the Czech Ministry of Education, Youth and Sports project No. LTAUSA18075.

References

[1] J.S. McCloy, M.J. Schweiger, C.P. Rodriguez, J.D. Vienna, Nepheline crystallization in nuclear waste glasses: progress toward acceptance of high-alumina formulations, Int. J. Appl. Glas. Sci. 2 (2011) 201–214.
[2] R.E. Gephart, A Short History of Hanford Waste Generation, Storage, and Release, PNNL-7 (States), (2003).
[3] J.D. Vienna, Nuclear waste vitrification in the United States: recent developments and future options, Int. J. Appl. Glas. Sci. 1 (2010) 309–321.
[4] Proposed shipment of commercial spent nuclear fuel to DOE national laboratories for research and development purposes (Supplemental Analysis) in, Office of Nuclear Energy, U.S. Department of Energy, 2015.
[5] A. Goel, J.S. McCloy, C.F. Windisch Jr., B.J. Riley, M.J. Schweiger, Carmen P. Rodriguez, J.M.F. Ferreira, Structure of rhenium-containing sodium borosilicate glass, Int. J. Appl. Glass Sci. 4 (2013) 42–52.
[6] B.J. Riley, J.S. McCloy, A. Goel, M. Liezers, M.J. Schweiger, J. Liu, C.P. Rodriguez, D.-S. Kim, Crystallization of rhenium salts in a simulated low-activity waste borosilicate glass, J. Am. Ceram. Soc. 96 (2013) 1150–1157.
[7] I. Pegg, Turning nuclear waste into glass, Phys. Today 68 (2015) 33–39.
[8] É. Vernaz, J. Bruezière, History of nuclear waste glass in France, Procedia Mater. Sci. 7 (2014) 3–9.
[9] M.T. Harrison, Vitrification of high-level waste in the UK, Procedia Mater. Sci. 7 (2014) 10–15.
[10] P. Sengupta, C.P. Kaushik, G.K. Dey, Immobilization of high-level nuclear wastes: the Indian Scenario, On a Sustainable Future of the Earth's Natural Resources, Springer, 2013, pp. 25–51.
[11] C.P. Kaushik, Indian program for vitrification of high-level radioactive liquid waste, Procedia Mater. Sci. 7 (2014) 16–22.
[12] W. Lutze, R.C. Ewing, Radioactive Waste Forms for the Future, Elsevier, 1988.
[13] C.H. Delegard, S.A. Jones, Chemical disposition of plutonium in Hanford site tank wastes, PNNL-23468-Rev. 1, Pacific Northwest National Laboratory Richland, Washington, United States, 2015.
[14] O.F. Hill, V.R. Cooper, Scale-up problems in the plutonium separations program, Ind. Eng. Chem. 50 (4) (1958) 599–602.
[15] G.J. Lumetta, B.K. McNamara, E.C. Buck, S.K. Fiskum, L.A. Snow, Characterization of high phosphate radioactive tank waste and simulant development, Environ. Sci. Technol. 43 (2009) 7843–7848.
[16] J.G. Reynolds, J.S. Page, G.A. Cooke, J. Pestovich, A scanning electron microscopy study of bismuth and phosphate phases in bismuth phosphate process waste at Hanford, J. Radioanal. Nucl. Chem. 304 (2015) 1253–1259.
[17] A.H. Bond, K.L. Nash, A.V. Gelis, J.C. Sullivan, M.P. Jensen, L. Rao, Plutonium mobilization and matrix dissolution during experimental sludge washing of bismuth phosphate, redox, and purex waste simulants, Sep. Sci. Technol. 36 (2001) 1241–1256.
[18] J.M. McKibben, Chemistry of the Purex process, Radiochim. Acta 36 (1984) 3–16.
[19] J.G. Reynolds, G.A. Cooke, J.S. Page, R. Wade Warrant, Uranium-bearing phases in Hanford nuclear waste, J. Radioanal. Nucl. Chem. 316 (2018) 289–299.
[20] G.L. Edgemon, V.S. Anda, H.S. Berman, M.E. Johnson, K.D. Boomer, History and operation of the Hanford high-level waste storage tanks, Corrosion 65 (2009) 163–174.
[21] J.C. Petrie, R.I. Donovan, R.E. Van der Cook, W.R. Christensen, Putting evaporators to work: vacuum evaporator–crystallizer handles radioactive waste, Chem. Eng. Prog. 72 (1976) 65–71.
[22] J.G. Reynolds, H.J. Huber, G.A. Cooke, J.A. Pestovich, Solid-phase zirconium and fluoride species in alkaline zircaloy cladding waste at Hanford, J. Hazard. Mater. 278 (2014) 203–210.
[23] J.G. Reynolds, G.A. Cooke, D.L. Herting, R. Wade Warrant, Salt mineralogy of Hanford high-level nuclear waste staged for treatment, Ind. Eng. Chem. Res. 52 (2013) 9741–9751.
[24] R. Wade Warrant, G.A. Cooke, Characterization of the solids waste in the Hanford waste tanks using a combination of XRD, SEM and PLM, Adv. X-Ray Anal. 46 (2003) 251–256.
[25] G.B. Barton, J.L. Hepworth, E.D. McClanahan, R.L. Moore, H.H. Van Tuyl, Chemical processing wastes. Recovering fission products, Indus. Eng. Chem. 50 (1958) 212–216.
[26] W.B. Barton, L.A. Gale, M.E. Johnson, Sixteen Years of Cesium Recovery Processing at Hanford's B Plant, Rockwell Hanford Operations, Richland, WA, 1986.
[27] D.S. Kim, M.J. Schweiger, C.P. Rodriguez, W.C. Lepry, J.B. Lang, J.V. Crum, J.D. Vienna, F. Johnson, J.C. Marra, D.K. Peeler, Formulation and Characterization of Waste Glasses with Varying Processing Temperature, PNNL-20774, Pacific Northwest National Lab. (PNNL), Richland, WA (United States), 2011.
[28] D.A. McKeown, H. Gan, I.L. Pegg, Raman and X-ray absorption spectroscopy studies of chromium–phosphorus interactions in high-bismuth high-level waste glasses, J. Nucl. Mater. 452 (2014) 526–532.
[29] D.A. McKeown, H. Gan, I.L. Pegg, X-ray absorption studies of bismuth valence and local environments in borosilicate waste glasses, J. Nucl. Mater. 420 (2012) 116–122.
[30] K.S. Matlack, Tests with High-Bismuth HLW Glasses, Washington, DC, Vitreous State Laboratory, The Catholic University of America, 2010 VSL-10R1780-1.
[31] J.D. Vienna, E.D. Collins, J.V. Crum, W.L. Ebert, S.M. Frank, T.G. Garn, D. Gombert, R. Jones, R.T. Jubin, V.C. Maio, J.C. Marra, J. Matyas, T.M. Nenoff, B.J. Riley, G.J. Sevigny, N.R. Soelberg, D.M. Strachan, P.K. Thallapally, J.H. Westsik, Closed Fuel Cycle Waste Treatment Strategy, No. INL/EXT-15-34504, Idaho National Lab. (INL), Idaho Falls, ID (United States), 2015.
[32] U.S. Department of Energy, Hanford tank waste retrieval, treatment, and disposition framework, (2013) Washington, D.C..
[33] D. Kim, Glass property models, constraints, and formulation approaches for vitrification of high-level nuclear wastes at the US Hanford Site, J. Korean Ceram. Soc 52 (2015) 92 90.
[34] P. Hrma, Melting of Foaming Batches: Nuclear Waste Glass, PNNL-SA-18408; CONF-9010253-1, Pacific Northwest Lab, Richland, WA (USA), 1990.
[35] W.S. Kuhn, Mathematical modeling of batch melting in glass tanks, in: H.L. Dieter Krause (Ed.), Mathematical Simulation in Glass Technology, Springer, Germany, 2002.
[36] M.K. Choudhary, Recent advances in mathematical modeling of flow and heat transfer phenomena in glass furnaces, J. Am. Ceram. Soc. 85 (2002) 1030–1036.
[37] M.K. Choudhary, R. Venuturumilli, M.R. Hyre, Mathematical modeling of flow and heat transfer phenomena in glass melting, delivery, and forming processes, Int. J. Appl. Glas. Sci. 1 (2010) 188–214.33.
[38] S. Lee, B.J. VanderVeer, P. Hrma, Z.J. Hilliard, J.S. Heilman-Moore, C.C. Bonham, R. Pokorny, D.R. Dixon, M.J. Schweiger, A.A. Kruger, Effects of heating rate, quartz particle size, viscosity, and form of glass additives on high-level waste melter feed volume expansion, J. Am. Ceram. Soc. 100 (2017) 583–591.
[39] D.R. Dixon, M.J. Schweiger, P.R. Hrma, Effect of Feeding Rate on the Cold Cap Configuration in a Laboratory-Scale Melter, United States: WM Symposia, Tucson, AZ, United States, 2013.
[40] D.R. Dixon, M.J. Schweiger, B.J. Riley, R. Pokorny, P. Hrma, Temperature distribution within a cold cap during nuclear waste vitrification, Environ. Sci. Technol. 49 (2015) 8856–8863.
[41] S. Lee, P. Hrma, R. Pokorny, J. Klouzek, B.J. VanderVeer, D.R. Dixon, S.A. Luksic, C.P. Rodriguez, J. Chun, M.J. Schweiger, A.A. Kruger, Effect of melter feed foaming on heat flux to the cold cap, J. Nucl. Mater. 496 (2017) 54–65.
[42] P.R. Hrma, A.A. Kruger, R. Pokorny, Nuclear waste vitrification efficiency: cold cap reactions, J. Non-Cryst. Solids 358 (24) (2012) 3559–3562.
[43] A.A. Kruger, P. Hrma, Effect of glass-batch makeup on the melting process, Ceramics-Silikaty 54 (3) (2010) 193–211.
[44] C. Chapman, Investigation of glass bubbling and increased production rate, REP-RPP-069, Rev. 0, Duratek, Richland, WA, 2004.
[45] J. Perez, C. Chapman, R. Mohr, K. Matlack, I. Pegg, Development and demonstration of an air bubbler design to meet high-level waste melter production rate requirements of the Hanford waste treatment and immobilization plant, Proceedings of the 10th International Conference on Environmental Remediation and Radioactive Waste Management, ICEM, 2005, pp. 1324–1331.
[46] R. Pokorny, A.A. Kruger, P. Hrma, Mathematical modelling of cold cap: effect of bubbling on melting rate, Ceramic-Silikaty 58 (4) (2014) 296–302.
[47] A.A. Kruger, K.S. Matlack, W.K. Kot, I.L. Pegg, I. Joseph, DM100 and DM1200 Melter Testing with High Waste Loading Glass Formulations for Hanford High Aluminum HLW streams, Test Plan 09T1690-1 No. ORP-44198, Hanford Site, Richland, WA (United States), 2009.
[48] A.A. Kruger, K.S. Matlack, W.K. Kot, I.L. Pegg, I. Joseph, C. Bardakci, H. Gan, W. Gong, M. Chaudhuri, Melt Rate Enhancement for High Aluminum HLW (High Level Waste) Glass Formulation Final Report 08R1360–1, Hanford Site, Richland, WA (United States), 2010.
[49] D.A. Pierce, P. Hrma, J. Marcial, B.J. Riley, M.J. Schweiger, Effect of alumina source on the rate of melting demonstrated with nuclear waste glass batch, Int. J.

Appl. Glas. Sci. 3 (2012) 59–68.
[50] K.S. Matlack, K. S., et al., Effect of the Form of Iron on HLW Melt Rate, Vitreous State Laboratory, The Catholic University of America, Washington, D.C, 2015.
[51] R. Pokorny, et al., Determination of temperature-dependent heat conductivity and thermal diffusivity of waste glass melter feed, J. Am. Ceram. Soc. 96 (2013) 1891–1898.
[52] J.A. Rice, R. Pokorny, M.J. Schweiger, P. Hrma, Determination of heat conductivity and thermal diffusivity of waste glass melter feed: extension to high temperatures, J. Am. Ceram. Soc. 97 (2014) 1952–1958.
[53] M. Hujova, R. Pokorny, J. Klouzek, D.R. Dixon, D.A. Cutforth, S. Lee, B.P. McCarthy, M.J. Schweiger, A.A. Kruger, P. Hrma, Determination of heat conductivity of waste glass feed and its applicability for modeling the batch-to-glass conversion, J. Am. Ceram. Soc. 100 (2017) 5096–5106.
[54] R. Pokorny, Z.J. Hilliard, D.R. Dixon, M.J. Schweiger, D.P. Guillen, A.A. Kruger, P. Hrma, One-dimensional cold cap model for melters with bubblers, J. Am. Ceram. Soc. 98 (2015) 3112–3118.
[55] S. Lee, P. Hrma, R. Pokorny, J.J. Traverso, J. Klouzek, M.J. Schweiger, A.A. Kruger, Heat transfer from glass melt to cold cap: effect of heating rate, Int. J. Appl. Glas. Sci. 10 (2019) 143–150.
[56] R. Pokorny, P. Hrma, Model for the conversion of nuclear waste melter feed to glass, J. Nucl. Mater. 445 (2014) 190–199.
[57] P. Hrma, R. Pokorny, S. Lee, A.A. Kruger, Heat transfer from glass melt to cold cap: melting rate correlation equation, Int. J. Appl. Glas. Sci. 10 (2019) 143–150.
[58] J. Chun, D.A. Pierce, R. Pokorny, P. Hrma, Cold-cap reactions in vitrification of nuclear waste glass: experiments and modeling, Thermochim. Acta 559 (2013) 32–39.
[59] W.H. Harris, D.P. Guillen, J. Klouzek, R. Pokorny, T. Yano, S. Lee, M.J. Schweiger, P. Hrma, X-ray tomography of feed-to-glass transition of simulated borosilicate waste glasses, J. Am. Ceram. Soc. 100 (2017) 3883–3894.
[60] K. Watanabe, et al., X-ray CT imaging of vitrified glasses containing simulant radioactive wastes: structure and chemical reactions of glass beads and wastes in the cold cap, Glass Technol.-Eur. J. Glass Sci. Technol. Part A 53 (2012) 273–278.
[61] D.P. Guillen, A.W. Abboud, R. Pokorny, W.C. Eaton, D. Dixon, K. Fox, A.A. Kruger, Development of a validation approach for an integrated waste glass melter model, Nucl. Technol. 203 (2018) 244–260.
[62] D.S. Kim, P. Hrma, Laboratory studies for estimation of melting rate in nuclear waste glass melters, Ceram. Trans.: Environ. Waste Manag. Issues Ceram. Indus. II 45 (1994).
[63] P.A. Smith, J.D. Vienna, P. Hrma, The effects of melting reactions on laboratory-scale waste vitrification, J. Mater. Res. 10 (1995) 2137–2149.
[64] I. Joseph, B.W. Brown, H. Gan, W.K. Kot, K.S. Matlack, I.L. Pegg, A.A. Kruger, High Aluminum HLW glasses for Hanford WTP, Hanford Site (HNF), Richland, WA (United States), 2009.
[65] K.M. Fox, D.K. Peeler, J.C. Marra, A. Aloy, R. Soshnikov, A. Trofimenko, J.D. Vienna, B.J. Riley, D. Kim, J.V. Crum, International studies of enhanced waste loading and improved melt rate for high alumina concentration nuclear waste glasses, Ceram. Trans. 207 (2009) 81–92.
[66] D.-S. Kim, M.J. Schweiger, W.C. Buchmiller, J. Matyas, Laboratory-scale melter for determination of melting rate of waste glass feeds, PNNL-21005; EMSP-RPT-012, Pacific Northwest National Laboratory (PNNL), Environmental Molecular Sciences Laboratory (EMSL), Richland, WA (US), 2012, pp. 1–50.
[67] I.M. Peterson, Y. Shi, D. Ma, J.L. Rygel, B. Wheaton, P.S. Whitfield, J. Wright, M. Carlineo, In situ measurements of reactions in a glass-forming batch by X-ray and neutron diffraction, J. Am. Ceram. Soc. 102 (2019) 1495–1506.
[68] Y. Doi, T. Yano, B.P. McCarthy, M.J. Schweiger, P. Hrma, Effects of particle size and briquetting of soda-lime-silicate glass batch on viscosity during batch-to-melt conversion, Int. J. Appl. Glas. Sci. 10 (2019) 115–124.
[69] Y. Doi, T. Maehara, T. Yano, Thermal diffusivity of soda–lime–silica powder batch and briquettes, Glass Technol. – Eur. J. Glass Sci. Technol. Part A 59 (2018) 92–104.
[70] B.P. McCarthy, J.L. George, D.R. Dixon, M. Wheeler, D.A. Cutforth, P. Hrma, D. Linn, J. Chun, M. Hujova, A.A. Kruger, R. Pokorny, Rheology of simulated radioactive waste slurry and cold cap during vitrification, J. Am. Ceram. Soc. 101 (2018) 5020–5029.
[71] M. Hujová, J. Klouzek, D.A. Cutforth, S. Lee, M.D. Miller, B. McCarthy, P.R. Hrma, A.A. Kruger, R. Pokorný, Cold-cap formation from a slurry feed during nuclear waste vitrification, Ceram. Int. 45 (2019) 6405–6412.
[72] A.A. Kruger, H. Gan, I.L. Pegg, W. Gong, C.C. Champman, I. Joseph, K.S. Matlack, Final report – High Level Waste vitrification system improvements, VSL-07R1010–1, Rev 0, dated 04/16/07, Hanford Site, Richland, WA (United States), 2013, pp. 1–278.
[73] K. Matlack, G. Diener, T. Bardakci, I. Pegg, Summary of DM1200 Operation at VSL – Final Report, The Catholic University of America, Vitreous State Laboratory, VSL-06R6710-2, Rev. 0, 2006.
[74] P. Hrma, C. Goles, D.D. Yasuda, Drainage of Primary Melt in a Glass Batch, PNL–SA– 18807, Pacific Northwest Laboratory, 1991.
[75] P. Hrma, L.M. Bagaasen, M.J. Schweiger, M.B. Evans, B.T. Smith, B.M. Arrigoni, D.-S. Kim, C.P. Rodriguez, S.T. Yokuda, J. Matyas, Bulk Vitrification Performance Enhancement: Refractory Lining Protection Against Molten Salt Penetration, PNNL-16773, Pacific Northwest National Laboratory (PNNL), Richland, WA (United States), 2007.
[76] L.M. Bagaasen, P.R. Hrma, D.-S. Kim, M.J. Schweiger, J. Matyas, C.P. Rodriguez, K.S. Witwer, Method to reduce molten salt penetration into bulk vitrification refractory materials, Proceedings of WM'08 Conference, Phoenix, AZ, 2008.
[77] L.M. Bagaasen, T.M. Brouns, M.L. Elliott, P.R. Hrma, D.-S. Kim, J. Matyáš, E.M. Pierce, B.P. McGrail, M.J. Schweiger, A. Beck, Transport of technetium and rhenium into refractory materials during bulk vitrification, Proceedings of WM'06 Symposia. WM-6312, Pacific Northwest National Laboratory, Richland, Washington, 2006.
[78] A.A. Kruger, C.P. Rodriguez, J.B. Lang, A.R. Huckleberry, J. Matyas, A.T. Owen, Crystal-tolerant glass approach for mitigation of crystal accumulation in continuous melters processing radioactive waste, ORP-52717, Hanford Site (HNF), Richland, WA (United States), 2012.
[79] J. Matyas, A. Huckleberry, C. Rodriguez, J. Vienna, A. Kruger, Empirical model for formulation of crystal-tolerant HLW glasses, Adv. Mater. Sci. Environ. Energy Technol. (2012) 121–126.
[80] J. Matyáš, D. Jansik, A. Owen, C. Rodriquez, J. Lang, A. Kruger, Impact of particle agglomeration on accumulation rates in the glass discharge riser of HLW melter, Ceram. Trans. 241 (2013) 59–69.
[81] C.M. Jantzen, K.G. Brown, Predicting the spinel–nepheline liquidus for application to nuclear waste glass processing. Part I: Primary phase analysis, liquidus measurment, and quasicrystalline approach, J. Am. Ceram. Soc. 90 (2007) 1866–1879.
[82] D.L. McClane, K.M. Fox, F.C. Johnson, J.W. Amoroso, A.A. Kruger, Dissolution of accumulated spinel crystals in simulated nuclear waste glass melts, J. Hazardous Toxic Radioact. Waste 22 (2018) 05018001.
[83] D.P. Guillen, A.W. Abboud, K. Fox, Particle settling in a simulated melter discharge riser, Mater. Lett. 236 (2019) 38–41.
[84] J. Matyas, J.D. Vienna, D. Peeler, K. Fox, C. Herman, A.A. Kruger, Roadmap for Development of Crystal-Tolerant High Level Waste Glasses, PNNL-23363, Pacific Northwest National Lab (PNNL), Richland, WA (United States), 2014.
[85] P. Hrma, B.J. Riley, J.V. Crum, J. Matyas, The effect of high-level waste glass composition on spinel liquidus temperature, J. Non-Cryst. Solids 384 (2014) 32–40.
[86] P. Hrma, Crystallization during processing of nuclear waste glass, J. Non-Cryst. Solids 356 (2010) 3019–3025.
[87] P. Hrma, Towards Optimization of Nuclear Waste Glass: Constraints, Property Models, and Waste Loading, SA-23384, Pacific Northwest Laboratory, Richland, WA, USA, 1994.
[88] J. Vienna, D. Kim, M. Schweiger, J. McCloy, J. Matyáš, G. Piepel, S. Cooley, Test Plan: Enhanced Hanford Waste Glass Models, US Department of Energy Report TP-EWG-00001, Revision (2013).
[89] A.A. Kruger, K. Matlack, W. Kot, I. Pegg, M. Chaudhuri, W. Lutze, Effects of High Spinel and Chromium Oxide Crystal Contents on Simulated HLW Vitrification in DM100 Melter Tests, VSL-09R1520–1, Rev. 0, Hanford Site, Richland, WA (United States), 2013.
[90] J. Klouzek, J. Alton, P.R. Hrma, T.J. Plaisted, Crucible Study of Spinel Settling in Molten High-Level Waste Glass, PNNL-SA-33010, Pacific Northwest National Laboratory, 2000.
[91] J. Matyáš, V. Gervasio, S.E. Sannoh, A.A. Kruger, Predictive modeling of crystal accumulation in high-level waste glass melters processing radioactive waste, J. Nucl. Mater. 495 (2017) 322–331.88.
[92] J.D. Vienna, Liquidus temperature-composition model for multi-component glasses in the Fe, Cr, Ni, and Mn spinel primary phase field, J. Non-Cryst. Solids 292 (2001) 1–24.
[93] M. Edwards, J. Matyáš, J. Crum, Real-time monitoring of crystal accumulation in the high-level waste glass melters using an electrical conductivity method, Int. J. Appl. Glas. Sci. 9 (2018) 42–51.
[94] N. Hutson, Letter Report on the Issue of Noble Metals in the DWPF Melter, WSRC-TR–2001-00337 REV. 0, Savannah River Site (United States) (2001).
[95] S.K. Sundaram, J.M. Perez, Noble Metals and Spinel Settling in High Level Waste Glass Melters, PNNL-13347, Pacific Northwest National Laboratory, Richland, WA (United States), 2000.
[96] H.D. Schreiber, F.A. Settle Jr., P.L. Jamison, J.P. Eckenrode, G.W. Headley, Ruthenium in glass-forming borosilicate melts, J. Less Common Metals 115 (1986) 145–154.
[97] J. Mukerji, S. Biswas, Oxidation states of ruthenium in glasses, Glass Technol. 12 (1971) 107–115.
[98] H. Shuto, T.H. Okabe, K. Morita, Ruthenium solubility and dissolution behavior in molten slag, Mater. Trans. 52 (2011) 1899–1904.
[99] O. Pinet, S. Mure, Redox behavior of platinum-group metals in nuclear glass, J. Non-Cryst. Solids 355 (2009) 221–227.
[100] M. Yamashita, H. Yamanaka, K.I. Sasage, Dissolution and separation of ruthenium in borosilicate glass, J. Am. Ceram. Soc. 87 (2004) 967–969.
[101] H. Boucetta, R. Podor, L. Stievano, J. Ravaux, X. Carrier, S. Casale, S.P. Gossé, A.L. Monteiro, S. Schuller, Mechanism of RuO_2 crystallization in borosilicate glass: an original in situ ESEM approach, Inorg. Chem. 51 (2012) 3478–3489.
[102] C. Krause, B. Luckscheiter, Properties and behavior of the platinum group metals in the glass resulting from the vitrification of simulated nuclear fuel reprocessing waste, J. Mater. Res. 6 (1991) 2535–2546.
[103] C.J. Capobianco, M.J. Drake, Partitioning of ruthenium, rhodium, and palladium between spinel and silicate melt and implications for platinum group element fractionation trends, Geochim. Cosmochim. Acta 54 (1990) 869–874.
[104] C. Simonnet, A. Grandjean, J. Phalippou, Electrical behavior of platinum-group metals in glass-forming oxide melts, J. Nucl. Mater. 336 (2005) 243–250.
[105] C. Simonnet, A. Grandjean, Mixed ionic and electronic conductivity of RuO_2–glass composites from molten state to glassy state, J. Non-Cryst. Solids 351 (2005)

1611–1618.
[106] R.D. Peters, Physical Modeling Studies of the HWVP Melter and an Alternate Design, HWVP-90-1.2.204.08A, Pacific Northwest National Laboratory, Richland, WA, 1990.
[107] H. Igarashi, The draining of noble-metals in vitrified nuclear waste by a melter with a sloping floor, Glass Technol. 32 (1991) 46.
[108] G.A. Jensen, A. Platt, G.B. Mellinger, W.J. Bjorklund, Recovery of noble metals from fission products, Nucl. Technol. 65 (1984) 305–324.
[109] K. Naito, T. Matsui, Y. Tanaka, Recovery of noble metals from insoluble residue of spent fuel, J. Nucl. Sci. Technol. 23 (1986) 540–549.
[110] S. Lee, H. Chung, Ion exchange characteristics of palladium and ruthenium from a simulated radioactive liquid waste, Sep. Sci. Technol. 38 (2003) 3459–3472.
[111] T. Suzuki, K. Morita, Y. Sasaki, T. Matsumura, Separation of Ru (III), Rh (III) and Pd (II) from nitric acid solutions using ion-exchange resins bearing carboxylic betaine, Sep. Sci. Technol. 51 (2016) 2815–2822.
[112] K. Singh, N. Sonar, T. Valsala, Y. Kulkarni, T. Vincent, A. Kumar, Removal of ruthenium from high-level radioactive liquid waste generated during reprocessing of spent fuel, Desalin. Water Treat. 52 (2014) 514–525.
[113] K. Motojima, Removal of ruthenium from PUREX process, J. Nucl. Sci. Technol. 26 (1989) 358–364.
[114] K. Uruga, K. Sawada, Y. Arita, Y. Enokida, I. Yamamoto, Removal of platinum group metals contained in molten glass using copper, J. Nucl. Sci. Technol. 44 (2007) 1024–1031.
[115] H. Jena, S. Raghavan, V. Pogaku, P.R. Bandi, G.K. Kuttanikkat Vadakkapet, Removal of Ru from simulated high-level waste prior to the final vitrification into borosilicate glass using tin as the alloying element: feasibility study, J. Hazardous Toxic Radioact. Waste 22 (2018) 04018018.
[116] J.G.H. Geeting, R.T. Hallen, Filtration, washing, and caustic leaching of Hanford tank AZ-101 sludge, Sep. Sci. Technol. 40 (2005) 1–15.
[117] C.P. McGinnis, T.D. Welch, R.D. Hunt, Caustic leaching of high-level radioactive tank sludge: a critical literature review, Sep. Sci. Technol. 34 (1999) 1479–1494.
[118] J.D. Vienna, D.-S. Kim, D.C. Skorski, J. Matyas, Glass Property Models and Constraints for Estimating the Glass To Be Produced at Hanford by Implementing Current Advanced Glass Formulation Efforts, PNNL-22631 Rev. 1; ORP-58289, Pacific Northwest National Laboratory (PNNL), Richland, WA (United States), 2013.
[119] J.D. Vienna, D.S. Kim, I.S. Muller, G.F. Piepel, A.A. Kruger, Toward understanding the effect of low-activity waste glass composition on sulfur solubility, J. Am. Ceram. Soc. 97 (2014) 3135–3142.
[120] I. Muller, H. Gan, K. Gilbo, I. Pegg, LAW Glass Property-Composition Models for K-3 Corrosion and Sulfate Solubility, VSL-15R3270–1, U.S. Department of Energy – Office of River Protection, Richland, WA, 2015.
[121] I. Muller, H. Gan, K. Gilbo, I. Pegg, K-3 Refractory Corrosion and Sulfate Solubility Enhancement, VSL-18R4360–1, U.S. Department of Energy – Office of River Protection, Richland, WA, 2018.
[122] D.A. McKeown, I.S. Muller, H. Gan, I.L. Pegg, W.C. Stolte, Determination of sulfur environments in borosilicate waste glasses using X-ray absorption near-edge spectroscopy, J. Non-Cryst. Solids 333 (2004) 74–84.
[123] D. Manara, A. Grandjean, O. Pinet, J.L. Dussossoy, D.R. Neuville, Sulfur behavior in silicate glasses and melts: implications for sulfate incorporation in nuclear waste glasses as a function of alkali cation and V_2O_5 content, J. Non-Cryst. Solids 353 (2007) 12–23.
[124] D.A. McKeown, I.S. Muller, H. Gan, I.L. Pegg, C.A. Kendziora, Raman studies of sulfur in borosilicate waste glasses: sulfate environments, J. Non-Cryst. Solids 288 (2001) 191–199.
[125] J.G. Reynolds, J.D. Belsher, A review of sodium fluoride solubility in water, J. Chem. Eng. Data 62 (2017) 1743–1748.
[126] K. Selkregg, Fusion cast refractories: roles of containment, Am. Ceram. Soc. Bull. 97 (2018) 21–28.
[127] C.M. Jantzen, K.J. Imrich, J.B. Pickett, K.G. Brown, High chrome refractory characterization: part II. Accumulation of spinel corrosion deposits in radioactive waste glass melters, Int. J. Appl. Glas. Sci. 6 (2015) 158–171.
[128] C.M. Jantzen, K.J. Imrich, K.G. Brown, J.B. Pickett, High chrome refractory characterization: part I. Impact of melt reduction/oxidation on the corrosion mechanism, Int. J. Appl. Glas. Sci. 6 (2015) 137–157.
[129] ASTM, Standard Test Methods for Determining Chemical Durability of Nuclear, Hazardous, and Mixed Waste Glasses and Multiphase Glass Ceramics: The Product Consistency Test (PCT), ASTM International, West Conshohocken, Pennsylvania, 2008.
[130] J.D. Vienna, J.O. Kroll, P.R. Hrma, J.B. Lang, J.V. Crum, Submixture model to predict nepheline precipitation in waste glasses, Int. J. Appl. Glas. Sci. 8 (2017) 143–157.
[131] H. Li, P. Hrma, J.D. Vienna, M. Qian, Y. Su, D.E. Smith, Effects of Al_2O_3, B_2O_3, Na_2O, and SiO_2 on nepheline formation in borosilicate glasses: chemical and physical correlations, J. Non-Cryst. Solids 331 (2003) 202–216.
[132] K. Fox, N. James, E. Tommy, B. David, R. Irene, W. Phyllis, Refinement of the Nepheline Discriminator: Results of a Phase I Study, WSRC-STI–2007-00659, SRS (US), Funding organization, US Department of Energy (United States), 2008.
[133] J.S. McCloy, N. Washton, P. Gassman, J. Marcial, J. Weaver, R. Kukkadapu, Nepheline crystallization in boron-rich alumino-silicate glasses as investigated by multi-nuclear NMR, Raman, & Mössbauer spectroscopies, J. Non-Cryst. Solids 409 (2015) 149–165.
[134] B.O. Mysen, P. Richet, Silicate Glasses and Melts: Properties and Structure, Vol. 10, Elsevier, 2005.
[135] H. Li, J. Vienna, P. Hrma, D. Smith, M. Schweiger, Nepheline Precipitation in High-Level Waste Glasses: Compositional Effects and Impact on the Waste Form Acceptability, MRS Online Proceedings Library Archive, 465, (1996).
[136] K.M. Fox, T.B. Edwards, D.K. Peeler, Control of nepheline crystallization in nuclear waste glass, Int. J. Appl. Ceram. Technol. 5 (2008) 666–673.
[137] A. Deshkar, Compositional dependence of crystallization in model high-level nuclear waste glasses, Ph.D thesis, Rutgers University, NJ, USA, 2019.
[138] P. Lu, S. Kapoor, L. Kobera, J. Brus, A. Goel, Impact of P_2O_5 on the structure and crystallization behavior of sodium- and alumina-rich model high-level nuclear waste glasses, 2019, (To be submitted).
[139] Y. Shaharyar, J.Y. Cheng, E. Han, A. Maron, J. Weaver, J. Marcial, J.S. McCloy, A. Goel, Elucidating the effect of iron speciation (Fe^{2+}/Fe^{3+}) on crystallization kinetics of sodium aluminosilicate glasses, J. Am. Ceram. Soc. 99 (2016) 2306–2315.
[140] M. Ahmadzadeh, J. Marcial, J. McCloy, Crystallization of iron-containing sodium aluminosilicate glasses in the $NaAlSiO_4$-$NaFeSiO_4$ join, J. Geophys. Res. Solid Earth 122 (2017) 2504–2524.
[141] A. Deshkar, M. Ahmadzadeh, A. Scrimshire, E. Han, P.A. Bingham, D. Guillen, J. McCloy, A. Goel, Crystallization behavior of iron-and boron-containing nepheline ($Na_2O{\cdot}Al_2O_3{\cdot}$ $2SiO_2$) based model high-level nuclear waste glasses, J. Am. Ceram. Soc. 102 (2019) 1101–1121.
[142] C.P. Rodriguez, J.S. McCloy, M. Schweiger, J.V. Crum, A.E. Winschell, Optical Basicity and Nepheline Crystallization in High Alumina Glasses, PNNL-20184; EMSP-RPT-003, Pacific Northwest National Laboratory, Richland, WA (United States), 2011.
[143] A. Deshkar, J. Marcial, S.A. Southern, L. Kobera, D.L. Bryce, J.S. McCloy, A. Goel, Understanding the structural origin of crystalline phase transformations in nepheline ($NaAlSiO_4$) based glass-ceramics, J. Am. Ceram. Soc. 100 (2017) 2859–2878.
[144] J. Vienna, B. Stanfill, G. Piepel, B. Riley, D. Kim, S. Cooley, J. Crum, T. Jin, C. Lonergan, 2016 Update of Hanford Glass Property Models and Constraints for Use in Estimating the Glass Mass to Be Produced at Hanford by Implementing Current Enhanced Glass Formulation Efforts, Pacific Northwest National Laboratory, Richland, WA, 2016.
[145] T.M. Besmann, K.E. Spear, Thermochemical modeling of oxide glasses, J. Am. Ceram. Soc. 85 (2002) 2887–2894.
[146] S.A. Utlak, T.M. Besmann, Thermodynamic assessment of the pseudoternary Na_2O–Al_2O_3–SiO_2 system, J. Am. Ceram. Soc. 101 (2018) 928–948.
[147] S.A. Utlak, T.M. Besmann, Thermodynamic assessment of the Na_2O-Al_2O_3-SiO_2-B_2O_3 pseudo-binary and-ternary systems, J. Chem. Thermodyn. 130 (2019) 251–268.
[148] J. Marcial, J. Kabel, M. Saleh, N. Washton, Y. Shaharyar, A. Goel, J.S. McCloy, Structural dependence of crystallization in glasses along the nepheline ($NaAlSiO_4$) – eucryptite ($LiAlSiO_4$) join, J. Am. Ceram. Soc. 101 (2018) 2840–2855.
[149] H.C. Palmer, K. Tazaki, W.S. Fyfe, Z. Zhou, Precambrian glass, Geology 16 (1988) 221–224.
[150] C.M. Jantzen, K.G. Brown, J.B. Pickett, Durable glass for thousands of years, Int. J. Appl. Glas. Sci. 1 (2010) 38–62.
[151] E.D. Zanotto, J.C. Mauro, The glassy state of matter: its definition and ultimate fate, J. Non-Cryst. Solids 471 (2017) 490–495.
[152] S. Gin, A. Abdelouas, L.J. Criscenti, W.L. Ebert, K. Ferrand, T. Geisler, M.T. Harrison, Y. Inagaki, S. Mitsui, K.T. Mueller, An international initiative on long-term behavior of high-level nuclear waste glass, Mater. Today 16 (2013) 243–248.
[153] B. Parruzot, P. Jollivet, D. Rebiscoul, S. Gin, Long-term alteration of basaltic glass: mechanisms and rates, Geochim. Cosmochim. Acta 154 (2015) 28–48.
[154] K. Ferrand, A. Abdelouas, B. Grambow, Water diffusion in the simulated French nuclear waste glass SON 68 contacting silica rich solutions: experimental and modeling, J. Nucl. Mater. 355 (2006) 54–67.
[155] D. Rebiscoul, F. Rieutord, F. Né, P. Frugier, R. Cubitt, S. Gin, Water penetration mechanisms in nuclear glasses by X-ray and neutron reflectometry, J. Non-Cryst. Solids 353 (2007) 2221–2230.
[156] H. Tomozawa, M. Tomozawa, Diffusion of water into a borosilicate glass, J. Non-Cryst. Solids 109 (1989) 311–317.
[157] B. Bunker, Molecular mechanisms for corrosion of silica and silicate glasses, J. Non-Cryst. Solids 179 (1994) 300–308.
[158] S. Gin, Open scientific questions about nuclear glass corrosion, Procedia Mater. Sci. 7 (2014) 163–171.
[159] T. Geisler, T. Nagel, M.R. Kilburn, A. Janssen, J.P. Icenhower, R.O.C. Fonseca, M. Grange, A.A. Nemchin, The mechanism of borosilicate glass corrosion revisited, Geochim. Cosmochim. Acta 158 (2015) 112–129.
[160] T. Geisler, A. Janssen, D. Scheiter, T. Stephan, J. Berndt, A. Putnis, Aqueous corrosion of borosilicate glass under acidic conditions: a new corrosion mechanism, J. Non-Cryst. Solids 356 (2010) 1458–1465.
[161] P. Van Iseghem, M. Aerstens, S. Gin, D. Deneele, B. Grambow, D.M. Strachan, B.P. McGrail, G.G. Wicks, Glamor-or how we achieved a common understanding on the decrease of glass dissolution kinetics, Ceram. Trans. 207 (2009) 115–126.
[162] S. Gin, J.V. Ryan, D.K. Schreiber, J. Neeway, M. Cabié, Contribution of atom-probe tomography to a better understanding of glass alteration mechanisms: application to a nuclear glass specimen altered 25 years in a granitic environment, Chem. Geol. 349 (2013) 99–109.
[163] P. Frugier, S. Gin, Y. Minet, T. Chave, B. Bonin, N. Godon, J.E. Lartigue, P. Jollivet,

A. Ayral, L. De Windt, G. Santarini, SON68 nuclear glass dissolution kinetics: current state of knowledge and basis of the new GRAAL model, J. Nucl. Mater. 380 (2008) 8–21.
[164] E. Curti, J.L. Crovisier, G. Morvan, A.M. Karpoff, Long-term corrosion of two nuclear waste reference glasses (MW and SON68): a kinetic and mineral alteration study, Appl. Geochem. 21 (2006) 1152–1168.
[165] G.S. Frankel, J.D. Vienna, J. Lian, J.R. Scully, S. Gin, J.V. Ryan, J. Wang, S.H. Kim, W. Windl, J. Du, A comparative review of the aqueous corrosion of glasses, crystalline ceramics, and metals, NPJ Mater. Degrad. 2 (2018) 15.
[166] J. Hopf, J.R. Eskelsen, M. Chiu, A.V. Ievlev, O.S. Ovchinnikova, D. Leonard, E.M. Pierce, Toward an understanding of surface layer formation, growth, and transformation at the glass–fluid interface, Geochim. Cosmochim. Acta 229 (2018) 65–84.
[167] S. Gin, M. Collin, P. Jollivet, M. Fournier, Y. Minet, L. Dupuy, T. Mahadevan, S. Kerisit, J. Du, Dynamics of self-reorganization explains passivation of silicate glasses, Nat. Commun. 9 (2018) 2169.
[168] S. Gin, P. Jollivet, M. Fournier, F. Angeli, P. Frugier, T. Charpentier, Origin and consequences of silicate glass passivation by surface layers, Nat. Commun. 6 (2015) 6360.
[169] M. Fournier, P. Frugier, S. Gin, Resumption of alteration at high temperature and pH: rates measurements and comparison with initial rates, Procedia Mater. Sci. 7 (2014) 202–208.
[170] M. Fournier, S. Gin, P. Frugier, Resumption of nuclear glass alteration: state of the art, J. Nucl. Mater. 448 (2014) 348–363.
[171] C.L. Trivelpiece, J.A. Rice, N.L. Clark, B. Kabius, C.M. Jantzen, C.G. Pantano, Corrosion of ISG fibers in alkaline solutions, J. Am. Ceram. Soc. 100 (2017) 4533–4547.
[172] S. Gin, L. Neill, M. Fournier, P. Frugier, T. Ducasse, M. Tribet, A. Abdelouas, B. Parruzot, J. Neeway, N. Wall, The controversial role of inter-diffusion in glass alteration, Chem. Geol. 440 (2016) 115–123.
[173] E. Vance, D. Gregg, I. Karatchevtseva, G. Griffiths, K. Olufson, G.J. Rees, J.V. Hanna, The influence of ZnO incorporation on the aqueous leaching characteristics of a borosilicate glass, J. Nucl. Mater. 494 (2017) 37–45.
[174] J. Hopf, S.N. Kerisit, F. Angeli, T. Charpentier, J.P. Icenhower, B.P. McGrail, C.F. Windisch, S.D. Burton, E.M. Pierce, Glass–water interaction: effect of high-valence cations on glass structure and chemical durability, Geochim. Cosmochim. Acta 181 (2016) 54–71.
[175] N. Godon, S. Gin, D. Rebiscoul, P. Frugier, SON68 glass alteration enhanced by magnetite, Proc. Earth Planet. Sci. 7 (2013) 300–303.
[176] A. Michelin, E. Burger, E. Leroy, E. Foy, D. Neff, K. Benzerara, P. Dillmann, S. Gin, Effect of iron metal and siderite on the durability of simulated archeological glassy material, Corros. Sci. 76 (2013) 403–414.
[177] L. Neill, S. Gin, T. Ducasse, T. De Echave, M. Fournier, P. Jollivet, A. Gourgiotis, N.A. Wall, Various effects of magnetite on international simple glass (ISG) dissolution: implications for the long-term durability of nuclear glasses, NPJ Mater. Degrad. 1 (2017) 1.